Metabolism of fatty acids and ketone bodies for glioblastoma growth: Implications for Ketogenic Diet Therapy

Jantzen Sperry[1], Janel E. Le Belle[2], Michael C. Condro[2], Lea Guo[2,3], Daniel Braas[4], Nathan Vanderveer-Harris[2], Kristen K.O. Kim[1], Whitney B. Pope[3], Ajit S. Divakaruni[1], Albert Lai[5,6], Heather Christofk[1,5,7,8], Harley I. Kornblum[1,2,5,8]

[1]Department of Molecular and Medical Pharmacology, David Geffen School of Medicine, University of California, Los Angeles, CA, 90095, USA, [2]Department of Psychiatry and Biobehavioral Sciences and Semel Institute for Neuroscience & Human Behavior, UCLA, [3]Department of Radiological Sciences, David Geffen School of Medicine, UCLA, [4]UCLA Metabolomics Center, UCLA, [5]Jonsson Comprehensive Cancer Center, UCLA, [6]Department of Neurology, UCLA, [7]Department of Biological Chemistry, UCLA, [8]Eli and Edythe Broad Center of Regenerative Medicine and Stem Cell Research, UCLA

ABSTRACT:

Glioblastoma (GBM) metabolism has traditionally been characterized by a dependence on aerobic glycolysis, prompting use of the ketogenic diet as a potential therapy. We observed growth-promoting effects on U87 GBM of both ketone body and fatty acid (FA) supplementation under physiological glucose conditions. An *in vivo* assessment of the unrestricted ketogenic diet surprisingly resulted in increased tumor growth and decreased animal survival. These effects are abrogated by FAO inhibition using knockdown of carnitine palmitoyltransferase 1 (CPT1). Primary patient GBM cultures revealed significant utilization of FAO regardless of tumorigenic

mutational status and decreased proliferation, increased apoptosis, and elevated mitochondrial ROS production with CPT1 inhibition. Metabolomic tracing with ^{13}C-labeled fatty acids showed significant FA utilization within the TCA cycle, indicating that FAO is used for both bioenergetics and production of key intermediates. These data demonstrate important roles for FA and ketone body metabolism that could serve to improve targeted therapies in GBM.

Running Title: Glioblastomas oxidize fatty acids and ketone bodies for growth

Financial Support: This work was supported in whole or part by National Institute of Health (NIH) Grants: NS052563 (H.I.K.) and CA179071 (A.L.) the UCLA SPORE in Brain Cancer (P50 CA211015); and the Dr. Miriam and Sheldon G. Adelson Medical Research Foundation (H.I.K.)

Corresponding Author: Harley I Kornblum

Room 379 Neuroscience Research Building

635 Charles E. Young Dr. South

Los Angeles, CA 90095

Tel: 310-794-7866

Fax: 310-206-5061

Email: HKornblum@mednet.ucla.edu

Conflicts of Interest: The authors disclose no potential conflicts of interest.

Total number of figures and tables: 8 Figures, 0 Tables.

INTRODUCTION:

Glioblastoma (GBM), the most aggressive and therapy resistant form of brain tumor, is traditionally characterized by its reliance on the Warburg effect. Under normal physiological conditions the healthy adult brain meets most of its energy demand by complete oxidation of glucose. This produces pyruvate which is then converted into acetyl-CoA for entrance into the TCA cycle to support the electron transport chain[1]. Thus, glycolysis and respiration remain tightly connected and result in more efficient ATP production with little lactic acid production. In contrast, the Warburg effect dramatically increases the rate of aerobic glycolysis and lactic acid production in the cytosol. While the benefits of this phenomenon are not completely understood, it has been posited that its main advantages are increased biomass production and facilitated invasion due to acidification of the microenvironment[2].

GBMs have been identified as highly reliant on aerobic glycolysis to the point that they are sometimes referred to as being “glucose addicted”. Several common signaling pathways found to be altered in GBM, such as PI3K-Akt-mTOR and Myc pathways, promote this phenotype by increasing expression of genes that allow cells to take up large amounts of glucose for increased glycolysis and lactate production[1, 3, 4]. Alterations to these pathways are often associated with mutations common to GBM such as EGFR and PTEN. EGFR, an activator of PI3K, is amplified in ~40% of GBMs with approximately half of those tumors expressing the constitutively active EGFRviii variant[5]. The tumor suppressor protein PTEN, a potent PI3K antagonist, is also altered in 30-40% of GBMs[6]. Similar to EGFR amplification, loss of PTEN function by either mutation or deletion results in hyperactivation of the PI3K/Akt signaling network. Despite these findings,

little progress has been made therapeutically in targeting enzymes reported to regulate glucose metabolism in GBM.

The interconnection between oncogenic signaling networks and metabolic pathways is complex in GBM. For example, while EGFR and PTEN mutations affect PI3K/Akt/mTOR activation, a major contributor to "glucose addiction", this signaling node also acts as a master regulator for switching between metabolic utilization of glucose, glutamine, fatty acids, and ketones[7,8,9,10]. Mutations in isocitrate dehydrogenases (IDH) 1 and 2 are also commonly found in gliomas. Wildtype metabolic function of these enzymes is primarily restricted to the TCA cycle where they produce alpha-ketoglutarate through the oxidative decarboxylation of isocitrate. However, these enzymes often incur neomorphic gain-of-function mutations that result in the production of 2-hydroxyglutarate (2-HG)[11], a proposed oncometabolite, along with widespread changes that extend far beyond the TCA cycle. The effects of IDH mutations have been attributed to altered glucose and nucleotide metabolism, DNA repair capacity, and reactive oxygen species (ROS) regulation, to name a few[12,13,14]. Thus, the mutations present in any given tumor (such as EGFR, PTEN, and IDH1) may determine the extent to which it can adjust to declining substrate availability, pathway inhibition, or therapeutic insult. Reconciling mutational status with metabolic flexibility represents a critical step to establishing more effective metabolic therapies for GBM.

The ketogenic diet (KD), which is a high fat, low carbohydrate, adequate protein diet has been proposed as a potential adjuvant therapy for a number of cancers including GBM[15,16]. With traditional diets, carbohydrates are plentiful and converted to glucose which then circulates to the brain as a major source of fuel. The KD limits carbohydrate availability and forces the production of ketone bodies such as ß-hydroxybutyrate and acetoacetate in the liver. Once in the brain, these

ketone bodies are converted to acetyl-CoA for entrance into the TCA cycle. The ability of the brain to oxidize ketone bodies is well-established, with one report estimating that up to 60% of the human brain energy requirement can be matched by ketone body oxidation[17]. The therapeutic premise of the KD is therefore dependent on the hypothesis that reducing glucose availability will starve cancer cells of necessary nutrients without causing harm to healthy brain tissue. The degree to which GBM cells can oxidize ketone bodies, however, is not completely understood, with several preclinical studies using the KD in animal brain tumor models showing varying levels of success[18, 19, 20].

Fatty acids (FAs) participate in a number of cellular processes including signal-transduction, membrane synthesis, and energy storage. FAs are typically synthesized from excess glucose and stored within the body as triglycerides in adipose tissue; however, they are also generated and stored endogenously by highly proliferative tissues like cancers through *de novo* FA synthesis. The elevated production of fatty acids in cancer is often driven by oncogenic mutations themselves[21]. Increased PI3K/Akt signaling, which can occur through mutations to EGFR or PTEN, results in upregulation of SREBP-1-mediated fatty acid synthesis and cholesterol uptake[22, 23, 24]. Similarly, oncogenic KRAS upregulates FA synthesis through mTORC1 and SREBP-mediated activation of fatty acid synthase (FASN)[25]. These FAs can then be used for membrane biosynthesis or as bioenergetic molecules. When cells require additional energy, FAs can undergo fatty acid beta-oxidation (FAO) within the mitochondria to generate acetyl-CoA to feed the TCA cycle and electron transport chain. In addition to ATP production, FAO also supports the production of a number of important cellular building blocks. For example, FA-derived citrate and malate can exit the TCA cycle to participate in the generation of both amino acid and lipid precursors[26]. FAO was largely overlooked in the brain until recently, likely due to long-standing

misconceptions that fatty acids (FAs) do not cross the blood brain barrier (BBB) and FAO does not take place. These misconceptions have since been dispelled and suggest that FAs play a significant role in overall brain metabolism[27, 28, 29, 30].

We and others[26, 31, 32] have established that glioblastoma cells oxidize FAs to promote proliferation and tumor growth. However, our study is the first to demonstrate this in multiple primary patient GBMs in addition to cell lines. We have found that there are only small differences in the level of FAO utilized by different lines, but that this isn't related to any known mutational status. It has been previously thought that mutations which promote PI3K/AKT/mTOR pathway signaling induce glucose addiction and a reliance on glucose metabolism[33], which we do not observe in our primary GBM cultures with mutations activating this pathway. This is dramatically confirmed by our *in vivo* trial of the ketogenic diet in animals with U87 GBM tumors which have high PI3K pathway activity due to a PTEN mutation. The premise of the ketogenic diet as an anti-tumor therapy is reliant on the hypothesis that lowering glucose availability will inhibit tumor growth. However, given the findings that GBM cells can readily utilize FAs as an energy source, the ketogenic diet could be thought of as a pro-growth diet for GBM. Indeed, this is what we found in our *in vivo* study where the diet significantly increased tumor size and lowered animal survival rates. We confirmed that this was due to the oxidative metabolism of FAs because its effects on tumor growth were impaired when the FA transport molecule CPT1A was knocked down. Functional studies and our own data using physiological glucose concentrations show that both fatty acids and ketone bodies are used by GBMs to a greater extent when compensating for decreased levels of glucose. This demonstrates that the metabolic reprogramming used by cancer cells allows them the flexibility to adapt to aversive microenvironmental conditions such as poor oxygenation or limited and variable nutrient availability. We used labeled FAs to demonstrate that

the oxidative utilization of FAs also supports a number of critical anabolic pathways throughout the GBM metabolome, as opposed to functioning solely in the production of ATP. Thus, by examining the utilization of alternative energy substrates in a large number of primary and tumor cell lines with different mutational statuses, we have now established that GBM metabolism is more universally adaptable than previously thought by promoting tumor growth via both catabolic and anabolic pathways simultaneously.

RESULTS:

Fatty acid and ketone oxidation in U87

In order to determine whether GBMs are capable of oxidizing fatty acids we first examined expression levels of CPT1, the rate-limiting enzyme required for FAO. Analysis of the TCGA dataset from primary GBM tumors reveals that of the three CPT1 isoforms found in humans, CPT1A and CPT1C are most highly expressed in GBM (Figure 1A). Western blot data also shows that CPT1A and C isoforms are expressed at similar levels in the U87 glioma cell line and primary human glioblastoma (gliomasphere) cell lines (Figure 5C). Inhibition of these enzymes with the CPT1-specific inhibitor etomoxir (ETOM) significantly diminished U87 cell growth (cell number) *in vitro* (Figure 1B). Because gliomasphere media used for *in vitro* studies contains high levels of glucose (25 mM) not found naturally in the human brain or in brain tumors, a glucose-limiting assay was performed to assess both fatty acid and ketone body utilization under more physiologically relevant glucose levels, with 2.5 mM glucose representing extracellular levels commonly found in the brain and 1 mM glucose serving as a low glucose condition to more closely mimic levels found in tissue that do not have adequate access to vascular supplies of glucose[34]. Palmitic acid supplementation (25-100 mM) partially rescued U87 cell growth under 2.5 mM low

glucose conditions (Figure 1C), whereas ketone supplementation with 2.5-5 mM 3-hydroxybutyrate (3-OHB) promoted cell growth in both 2.5 mM and 1 mM glucose (Figure 1D). Neither FA nor ketone supplementation had growth-promoting effects under non-physiological conditions of high glucose (25 mM).

To further determine how and where FAs are utilized within U87 cells, untreated CNTL cells, cells treated with ETOM, and cells with CPT1A knockdown were subjected to LC-MS metabolomic analysis using fully-labeled ^{13}C palmitic acid in physiological glucose conditions (2.5 mM). Analyzing fractional contribution (or the percent of labeled carbons for each metabolite) within these samples revealed labeling throughout the TCA cycle as well as in the ubiquitously important currency metabolite ATP. Treatment with ETOM or CPT1A knockdown dramatically diminished this labeling (Figure 2A). Similar effects were observed when analyzing the relative amounts of these metabolites, wherein ETOM treatment and CPT1A knockdown significantly decrease levels of TCA-associated metabolites, acetyl-CoA, and ATP (Figure 2B). Taken together these data confirm FAO utilization while also suggesting that of the 3 CPT1 isoforms, CPT1A appeared to be the primary isoform regulating this process in GBM.

CPT1A knockdown and the ketogenic diet

Based on these initial results and previous studies[35, 36] that have indicated that many brain tumors may lack the ability to oxidize ketones as an energy substrate, we sought to determine if inhibiting FAO while concurrently implementing a ketogenic diet using an orthotopic xenograft model in mice might serve as an effective therapeutic strategy. It is thought that this strategy would reduce the availability of glucose as an energy substrate and make the GBM cells more vulnerable to cell death (starvation) by also inhibiting FAO as an alternative energy source. Because

expression data indicated that CPT1A is most highly expressed in GBM, lentiviral shRNAs were used to knockdown CPT1A in U87 cells expressing firefly luciferase-GFP (Fluc-GFP). While this did not result in complete knockdown, the degree of knockdown was sufficient to significantly inhibit *in vitro* cell growth by ~40% to levels near what was observed with ETOM alone (Figure 3A), once again suggesting that CPT1A is the primary isoform regulating FAO in these cells. This also demonstrates the importance of endogenous fatty acid oxidation to the maintenance of normal *in vitro* cell growth in these GBM cells despite U87s having a PTEN mutation which increases PI3K/AKT/mTOR signaling, which has been previously thought to inhibit FAO in GBM. To assess these results *in vivo* as well as to determine the effectiveness of the KD on tumor growth, U87 cells (shCNTL and shCPT1A) were injected into the striatum of adult NSG mice. On day 4, half of each group was switched to a calorie-unrestricted KD followed by weekly bioluminescent imaging with luciferin as shown in Figure 3B. At 21 days post-injection, animal weights, blood glucose levels, and blood ketone levels were evaluated. Both of the ketogenic diet cohorts (shCNTL and shCPT1A) exhibited decreased total body weight, decreased blood glucose levels, and increased blood 3-hydroxybutyrate levels, confirming ketosis was achieved in these animals (Figure 3 C-E). Contrary to our initial hypothesis, analysis from weekly bioluminescent imaging shows that the shCNTL cohort receiving the KD had the greatest percent increase in tumor size, but that this increased growth was abrogated by CPT1A knockdown (Figure 4A). A similar experiment using a CPT1A CRISPR/Cas9 system corroborated the finding that the KD promoted U87 tumor growth, but that this could be overcome by CPT1A-mediated FAO inhibition (Supplementary Figure 1). These findings were mirrored by analysis of mouse survival. The poorest survival was observed in the shCNTL group receiving the KD and the greatest in the shCPT1A group receiving standard chow. (Figure 4B). Immunohistochemisty of sectioned post-

mortem tissue confirmed that CPT1A knockdown was maintained throughout the length of the experiment (Figure 4C). Knockdown of CPT1C in U87 had inhibitory growth effects *in vitro*, albeit not to the degree of CPT1A knockdown, but there were no observable differences in tumor growth *in vivo* when compared to shCNTL cells (Supplementary Figure 2). The findings using our model, while surprising, may indicate a previously unknown ability of GBM cells to thrive under ketosis while also highlighting an important role of CPT1A-mediated FAO in regulating this process.

Primary GBM gliomasphere cultures

While U87 cells are a reasonable model to test biochemical hypotheses in GBM, the cells bear significant differences from primary GBM cells. In order to confirm the potential importance of fatty acid oxidation in GBM we examined the potential of primary gliomasphere cultures to oxidize FAs and ketone bodies to support growth and cell survival. Analysis of our gliomasphere microarray dataset[37] was performed to determine whether our primary cultures express the CPT1 isoforms, similar to that of tumors (Figure 1A). This analysis revealed once again that CPT1A and CPT1C were more highly expressed than CPT1B (Figure 5A). Protein expression of these isoforms was confirmed using Western blot and immunocytochemistry. Respiration using palmitoyl-CoA as a substrate in primary GBM lines confirmed that CPT1-mediated FAO occurred in these cells (Figure 5B).

While other studies have utilized ETOM up to millimolar concentrations, more recent research indicates that 3 μM ETOM is sufficient to fully inhibit CPT1 activity in macrophages, with excessive concentrations resulting in off-target effects[38]. The concentration of ETOM required to fully saturate CPT1 activity in GBM has not yet been established, however, so we

sought to address this issue by analyzing differences between 3 μM and 100 μM ETOM on basal oxygen consumption rates. The higher dose slightly decreased oxygen consumption in two of the cell lines, suggesting a potential off-target effect of 100 μM ETOM (Figure 5C). However, further analysis using palmitic acid and ETOM clearly demonstrated that GBM cells are able to actively oxidize both endogenous and exogenous FAs (Figure 5D). We also assessed the ability of a primary GBM (HK157) to utilize exogenously supplied FA and 3-OHB as an energy substrate to support cellular growth in both physiological and high glucose conditions (Figures 5E-F). Similar to what was observed in U87 cells, both exogenously supplemented FA and 3-OHB had growth-promoting effects under lower and more physiologically relevant glucose levels (2.5 mM), demonstrating the ability of the primary GBM to utilize alternative substrates.

To further assess inhibition of endogenous FAO on GBM cell growth and survival we tested the effects of ETOM in a panel of primary GBM cultures. These experiments were initially done under high glucose, non-FA supplemented conditions. A 7-day treatment with ETOM resulted in diminished overall culture growth for all gliomasphere lines tested (Figure 6A). This analysis yielded no significant differences with regard to IDH1 mutant status, PTEN deficiency, EGFR amplification, or the presence of the EGFRviii mutation (data not shown). Interestingly, ETOM treatment did not inhibit the growth of cultured human fetal neurospheres or SVZ-derived mouse neurospheres. This may indicate that FAO is GBM-specific, irrespective of mutational status, and less important to healthy tissue making it a potentially attractive therapeutic target. Following a 4-day treatment with ETOM we found a significant decrease in actively dividing cells as assessed using bromodeoxyuridine (Brdu) incorporation (Figure 6B), demonstrating the importance of endogenous FAO to the maintenance of cell proliferation even in GBMs (HK301) with a mutation that enhances AKT pathway signaling. In addition to these effects on proliferation

we also observed an increase in cell death as measured by annexin V/propidium iodide staining (FACS) following treatment with ETOM (Figure 6C). Analysis of ETOM treatment on intracellular reactive oxygen species (ROS) levels revealed no change in total intracellular ROS. Treatment did increase mitochondrial superoxide levels across all lines tested (Figure 6D) suggesting that etomoxir, which binds to CPT1 on the outer mitochondrial membrane, specifically alters ongoing FA mitochondrial oxidative metabolism. A 7-day growth assay in a number of primary GBM lines of varying mutational status was performed in 2.5 mM glucose, representative of physiological levels. This showed a slight increase in sensitivity to ETOM inhibition of endogenous FAO than what was observed in 25 mM glucose (Figure 6E). We also assessed the ability of the primary GBMs to utilize exogenously supplied FA and 3-OHB as an energy substrate to support cellular growth at 2.5 mM glucose (Figure 6E). Our results indicate that there is increased variability in the ability of the cells to promote cell growth from what was observed in the U87 glioma cell line (Figure 1C-D), likely representing a heterogeneity among GBMs to utilize these alternative substrates in place of glucose. Taken together, these data support our hypothesis that FAO is a significant contributor to overall GBM metabolism and growth, which is not prevented by PI3K/AKT/mTOR pathway-promoting mutations in our lines as has been observed in previous studies on GBM glucose dependency and fatty acid utilization[39, 33, 40].

LC-MS with fully-labeled palmitic acid

We utilized LC-MS analysis with fully-labeled ^{13}C palmitic acid to characterize the contribution of FAO to the metabolome of primary GBM cells. Fractional contribution studies revealed that ETOM treatment caused widespread changes in carbon labeling across the metabolome (Figure 7A). Importantly, ETOM resulted in diminished labeling of acetyl-CoA, the

end product of FAO, along with an increase in the amount of labeled palmitate within the cell (Figure 7B). Both results confirmed that labeled FAs were taken up and oxidized within the cell. In addition to acetyl-CoA, ETOM treatment also resulted in diminished labeling within the TCA cycle and among metabolites that commonly feed into the TCA cycle such as glutamine, glutamate, and lactate (Figure 7B). Analysis of the relative amounts of metabolites with ETOM treatment did not result in changes to overall acetyl-CoA or palmitate levels. However, ETOM treatment did result in lower relative levels of TCA-associated metabolites which include alpha-ketoglutarate, citrate, fumarate, glutamine, and glutamate (Figure 7C). A full list of significantly altered metabolites resulting from FAO inhibition with ETOM (Supplementary Table 1) demonstrates that GBM cells utilize FAO to support a number of critical metabolic pathways throughout the GBM metabolome.

Fatty acid oxidation in IDH1 mutant GBM

Recent studies, including one from our own group[12], have demonstrated that GBMs harboring an isocitrate dehydrogenase 1 (IDH1) mutation represent a metabolically distinct subset of glioma. Because of this, we sought to identify potential differences in FAO utilization between our IDH1 mutant and IDH WT gliomasphere cultures. Analysis of microarray data from 67 gliomasphere lines, 7 of which are IDH1 mutant, revealed elevated mRNA expression of CPT1A in IDH1 mutant lines (Figure 8A) compared to IDH wildtype cultures. Western blot analysis confirmed elevated CPT1A protein expression (Figure 8B). Similar to IDH WT cells, LC-MS analysis with fully-labeled palmitic acid in an IDH1 mutant cell line showed diminished labeling of acetyl-CoA and several TCA-associated metabolites when treated with ETOM (Figure 8C). Interestingly, 2-hydroxyglutarate (2-HG), a proposed oncometabolite and the resulting product of

the IDH1 mutant enzyme itself, was among the most heavily labeled metabolites in this particular IDH1 mutant line. Treatment with ETOM significantly diminished both the fractional contribution and relative amount of intracellular 2-HG, suggesting that FAO may serve as a major contributor to 2-HG production in IDH1 mutant GBMs (Figure 8C-D). FAO inhibition with ETOM in IDH1 mutant cells did not result in a decrease in the relative amounts of TCA cycle intermediates as was observed in IDH WT cells (Figure 8D, Supplementary Figure 3), perhaps indicating a greater reliance on FAO to feed the TCA cycle in IDH WT GBM. Analysis of the full list of significantly different metabolites revealed fewer overall metabolites altered by ETOM treatment in IDH1 mutant cells (Supplementary Table 2). These data confirm FAO utilization in both IDH1 mutant and wildtype cells while highlighting several potentially important metabolic differences between the two. Further investigation with a greater number of IDH mutant and wildtype lines will be needed to fully elucidate these differences.

DISCUSSION

Identifying metabolic vulnerabilities in cancer for use in targeted therapies has been a topic of interest for decades. While glucose metabolism has drawn the most attention in the scientific community, the ability of brain tumor cells to utilize other substrates for cellular maintenance and to meet bioenergetic demands has become increasingly evident[41, 10, 42, 43]. Several lines of evidence exist for the use of a ketogenic diet (KD) to treat brain tumors based on the idea that cancers are highly glycolytic and reducing the availability of blood glucose leaves the cells vulnerable to metabolic and chemotherapeutic insult. The first lies with the innate ability of the human body to efficiently adapt to ketosis[44]. For example, the KD has been successfully implemented to treat certain diseases such as refractory pediatric epilepsy with no clear sustained adverse health

effects[45, 46, 47]. Additionally, several previous studies have indicated that many brain tumors may lack the ability to oxidize ketones due to decreased expression of several mitochondrial genes required to do so[35, 36], although there is also evidence suggesting gliomas oxidize ketone bodies at comparable levels to the brain when exposed to a KD[48]. Our study shows that as glucose levels are diminished, GBM cells can adapt by at least partially shifting their metabolism to accommodate ketone body oxidation. Prior animal studies investigating the therapeutic potential of the KD have yielded mixed results, usually depending on the manner of administration and ability to achieve ketosis[18, 20, 49, 50]. One study using U87 cells in a mouse tumor model found that an *ad libitu*m KD resulted in increased blood ketone levels without affecting blood glucose or tumor growth[20]. Only with a calorie-restricted KD were glucose levels and tumor growth diminished. This is consistent with other studies demonstrating anti-tumor effects of calorie restriction irrespective of the KD[43, 51, 52]. Here we report that the *ad libitum* KD, albeit of a slightly different formulation and longer period of administration, significantly elevated blood ketone levels, decreased blood glucose, but resulted in increased tumor growth. While it is possible that the KD can have some therapeutic utility depending on its implementation, our data suggest that clinical trials investigating such treatments need to proceed with a great deal of caution[19, 53, 54, 55].

In addition to ketone body metabolism, this study also focused on the ability of GBMs to oxidize FAs. Building upon previous reports[26, 31, 56], our results demonstrate that both GBM cell lines and primary patient GBM cell cultures express the necessary enzymes required for FAO, they utilize FAs to support overall metabolism, and that inhibition of this process has anti-proliferative effects. Importantly, our results also suggest that the ability to oxidize FAs may be intrinsic to GBM and is not directly counteracted by EGFR amplification, constitutive activation (EGFRviii mutation), or PTEN mutations. Activation of the PI3K/Akt/mTOR pathway has been implicated

in glucose addiction, a diminished ability to utilize alternative substrates that leaves malignant cells particularly vulnerable to glucose starvation[57, 58], and a metabolic shift towards FA synthesis[22]. However, our current study suggests that under physiologically relevant glucose conditions (2.5 mM), FAs play a central role in the overall GBM metabolome regardless of mutational status, as shown through the use of multiple primary GBM cell lines. Our findings of a mutation-independent use of FAO may be due to methodological differences with previous studies, such as our use of physiological glucose levels, or lower ETOM concentrations to limit off-target effects. Furthermore, our surprising *in vivo* findings that show an increase in U87 tumor growth with a ketogenic diet support our *in vitro* findings that Akt-enhancing mutations do not make GBMs "glucose addicted", as U87 cells themselves are PTEN deficient. The ketogenic diet limits the availability of glucose to the tumor *in vivo,* so the enhanced tumor growth we observed must have been supported by the use of alternative energy substrates despite U87s having PTEN mutations.

FAO by these tumors may at first glance seem counterintuitive since the brain receives an ample supply of glucose, the most highly utilized substrate in GBM. ATP generation by FAO also demands more oxygen, is a slower overall process, and generates more superoxide than glycolysis[59]. While the idea of simultaneous FA synthesis and oxidation seems counterproductive, studies such as this make it increasingly clear that the ability to oxidize FAs make malignant cells more resilient and adaptable to conditions of metabolic stress. FAs represent a readily available and easily stored substrate that can be utilized to support both bioenergetic demands and as a raw material for the production of other cellular components. In malignant glioma tumors, lipid levels have been reported to be higher compared with normal brain tissues [60]. Gliomas can both produce free FAs and lipid stores endogenously via *de novo* synthesis from excess glucose and via uptake

of exogenously produced free fatty acids from blood. Our experiments suggest that both endogenous and exogenous sources of FAs can be used as an energy substrate to support cell growth in GBMs. Perhaps the most notable aspect of FAO is that it results in the production of acetyl-CoA, an important metabolite that regulates a number of cellular processes including the TCA cycle. Recent evidence demonstrates that much of the acetyl-CoA produced by malignant gliomas is derived from sources other than glucose[61], highlighting FAO as a potentially critical contributor to overall brain tumor metabolism. Our ^{13}C-labeled FA tracing experiments support this finding while also demonstrating that in addition to feeding into the TCA cycle, FAO contributes extensively to anabolic pathways throughout the GBM metabolome.

A recent study published during the preparation of this manuscript reported that GBMs are reliant on FAO to sustain proliferation and that acyl-CoA binding protein (ACBP) promotes this process by regulating the availability of long chain fatty-acyl CoAs to the mitochondria[32]. This group also concluded that FAO was the preferred pathway for oxidative phosphorylation even in the presence of glucose. Our results build upon these findings by identifying CPT1A as a valid therapeutic target for GBM and demonstrating that inhibition of CPT1-mediated FAO results in decreased tumor growth and improved survival using a murine orthotopic xenograft model. We identified that CPT1A knockdown effectively inhibited GBM tumor growth independent of dietary manipulation or glucose availability. While the KD initiates production of ketone bodies such as beta-hydroxybutyrate, it also results in increased FA availability with the potential to be taken up and utilized by the tumor[62, 63]. Because CPT1A knockdown nullified the observed increase in tumor growth from the KD, our results implicate FAs, rather than ketone bodies, as the primary metabolic substrates responsible for the surprising growth-promoting effects of the ketogenic diet. These results provide strong evidence that FAO is a significant pathway in GBM and may serve

as a valuable therapeutic target either alone or in combination with other currently investigated treatments.

While investigating FA metabolism in GBM as a whole, we also sought to characterize potential differences in FAO utilization between IDH1 mutant and wildtype GBM cells. Recent evidence suggests that GBMs harboring IDH mutations represent a distinct subclass of glioma[64]. Our group previously demonstrated that IDH1 mutant gliomaspheres are metabolically distinguishable from their WT counterparts based on expression profiles, glucose consumption, and nucleotide synthesis utilization[12]. The results of this study suggest further metabolic differences in IDH mutant GBM cells with regard to FAO. Analysis of CPT1-isoform expression revealed increased expression of CPT1A in IDH1 mutant cultures relative to IDH wildtype cells. LC-MS tracing experiments with ^{13}C-palmitic acid revealed extensive FA utilization throughout the metabolomes of both IDH mutant and WT cells. However, the effects of FAO inhibition with ETOM was more pronounced within the TCA cycle of IDH WT cells. Importantly, 2-HG was among the most heavily labeled metabolites in IDH mutant cells. Treatment with ETOM significantly decreased both the fractional contribution and relative amount of 2-HG, indicating FAs may serve as a vital component for the production of this proposed oncometabolite. While these effects were only tested in a single IDH1 mutant cell line, and thus require further investigation, our results suggest FAO represents an additional mechanism contributing to the unique metabolic phenotype of IDH mutant gliomas.

Although our findings emphasize the complex and highly adaptable nature of brain tumor metabolism, important aspects of these studies require further investigation. The preponderance of evidence reported in this study support the conclusion that GBMs oxidize FAs. Inhibition of FAO with ETOM resulted in overall deficits in cellular growth and FA-mediated mitochondrial

respiration. Meanwhile, FA supplementation under physiologically relevant glucose concentrations demonstrated inverse effects to that of ETOM. Our LC-MS studies also clearly show that FAs are taken up, oxidized, and utilized throughout the GBM metabolome. Finally, many of the effects of FAO inhibition achieved with ETOM were validated using multiple methods of CPT1A knockdown. The fact that etomoxir has been shown to exhibit off-target effects in certain cells at high doses cannot be overlooked, however. Developing more potent and specific FAO inhibitors, perhaps even for individual CPT1 isoforms, could prove essential for targeting brain tumors in patients. Due to the grim prognosis associated with glioma and the currently inadequate treatment options available, this study highlights several important aspects of brain tumor metabolism that have direct application to improving current standard of care therapy.

METHODS:

Collection and Maintenance of *In Vitro* Cultures

Tumor samples were collected under institutional review board-approved protocols and graded by neuropathologists. Primary gliomasphere cultures were prepared as follows. Immediately after receiving resected tissue, samples were digested with papain and acellular debris was removed. Those cells which remained were incubated in gliomasphere defined media containing DMEM/F12 supplemented with B27, heparin, EGF, bFGF, and penicillin/streptomycin until sphere formation was achieved. Gliomasphere stocks were frozen down at approximately passage 5 to maintain cells at low passage throughout the study. All cell lines used in this study, including U87, were continuously grown in serum-free gliomasphere media.

Expression Analysis

Relevant expression, mutational status (such as EGFR and IDH1), and patient characteristics for the majority of cell lines used in this study have been previously reported[37,12]. The following cultures are known to be PTEN deficient (U87, HK217, HK229, HK296, HK301) but there may be other cultures that are PTEN mutated/deleted as well. Also of note, while BT142 is IDH1 mutant (R132H), it does not produce 2-HG. HK211 is both IDH1 (R132H) and EGFRviii mutant. Known status of EGFR, PTEN, and IDH1 are indicated in Figure 6A for primary GBM cultures. Analysis of CPT1-isoform expression is based on the microarray dataset (GSE98995) previously described by Laks et al. 2016 and available in the Gene Expression Omnibus (GEO) repository.

Variable Glucose Media and Substrate Supplementation

All media described contain B27, heparin, EGF, bFGF, and penicillin/streptomycin. For 25 mM glucose the base media used is Neurobasal-A Medium ([-] Glutamine) (Gibco #10888-022) supplemented with GlutaMax Supplement (Gibco #35050061). 2.5 mM and 1 mM glucose media was made by combining the Neurobasal-A Medium ([-] Glutamine) above with Neurobasal-A Medium ([-] D-glucose, [-] Sodium Pyruvate) (Gibco #A24775-01) to achieve the desired glucose concentration. Glutamax Supplement and sodium pyruvate (Gibco #11360-070) were then added to reach a final concentration of 1X. Palmitic acid was purchased from Sigma-Aldrich (#P0500) and conjugated with fatty acid free, low endotoxin bovine serum albumin (BSA, Sigma Aldrich, #A1595). Carnitine (Sigma Aldrich, #C0283) was included in fatty acid-supplemented conditions. 3-hydroxybutyrate (3-OHB) was also purchased from Sigma (#166898).

shRNA and CRISPR/Cas9 Lentiviral Knockdown

Plasmids with shCPT1A (RHS4531-EG1374 glycerol set), shCPT1-C (RHS4531-EG126129 glycerol set), and the non-silencing shCNTL (RHS4346) cloned into pGIPZ expression vectors were purchased from Dharmacon. The firefly luciferase-GFP virus Fluc-GFP (backbone= pRRL-sinCMV-iresGFP) was produced by UCLA Vectorcore and supported by Molecular Technologies Core (IMTC) CURE/P30 DK41301-26. These plasmids were transfected into 293T cells along with 1st generation viral ΔR8.74 package and VSV-g envelope for production of lentivirus. For CRISPR experiments the following plasmids were used: CPT1A-validated CRISPR guideRNA (Edigene SG00441287A), LentiCas9-EGFP (Addgene 63592), and pgRNA-humanized plasmid, (Addgene 44248). Each plasmid was used to generate three separate lentiviruses as described above. For CPT1A-CRISPR knockdown experiments cells were then infected sequentially: first with either the CPT1A guideRNA or pgRNA-humanized (CNTL) virus, and then with the LentiCas9-EGFP virus. Cells expressing both fluorophores for the guideRNA and Cas9 were selected for by fluorescence. Those selected cells were then plated at clonal density and expanded to achieve a more uniform population expressing both the guideRNA and Cas9 vectors.

U87 In Vivo Orthotopic Xenotransplants

All animal experimentation was performed with institutional approval following NIH guidelines using adult NSG mice. Intracranial xenotransplants were performed similarly to previous descriptions with minor changes[65].

CPT1A /Ketogenic Diet:

One hundred thousand U87 cells expressing firefly luciferase-GFP (Fluc-GFP) along with either shCNTL or shCPT1A plasmids were stereotactically injected into the striatum of non-obsese

diabetic gamma null (NSG) mice under isoflurane anesthesia over 5 minutes using the following coordinates: 1.5 mm lateral to and -0.5 mm anterior to Bregma, and 3.0 mm below the pial surface. N= 10 mice per group. As shown in Figure 3B, mice were kept on standard chow for 4 days to allow appropriate recovery, after which half of each group was placed on the ketogenic diet (BioServ, S3666). On Day 8, weekly bioluminescence imaging was initiated as described below. On Day 21 mouse weight, blood glucose and ketone measurements were taken. Tumor growth was measured until each animal either died or became morbid. Mouse survival was tracked for all groups. This experimental design was also implemented for CPT1A CRISPR/Cas9 transplants.

CPT1-C Transplants:

Transplants for this experiment were carried out as described above with the exception that the ketogenic diet was not implemented and therefore only 20 total mice were used (10 per group). *In vivo* tumor studies were conducted in immunosuppressed mice using the U87 malignant glioma cell line. This cell line was used because of its experimental consistency, similar FAO profile to primary GBM lines, and its ability to establish tumors quickly. The speed of tumor formation was important, not simply for convenience, but it allowed us to take into account concerns regarding significant weight loss and the overall health of animals receiving a long-term ketogenic diet.

Bioluminescent Imaging

Optical imaging was performed at the Preclinical Imaging Technology Center at the Crump Institute for Molecular Imaging at UCLA. 100 µl of D-luciferin (GoldBio) dissolved in phosphate buffer saline without Ca2+ or Mg2+ (30 mg/ml) was introduced to each animal by intraperitoneal (IP) injection. After 7 minutes of conscious uptake, mice were anesthetized by inhalation of 2.6% isoflurane in oxygen and placed in dedicated imaging chambers. The IVIS Lumina 2 imaging

system (Caliper Life Sciences) was utilized for *in vivo* bioluminescent imaging. A corresponding photograph of the mice was taken and co-registered with the luminescent image for signal localization. Images were analyzed by drawing regions of interest and quantified as total flux (photons/second) with the Living Image software package (Perkin Elmer).

Western Blot and Immunohistochemistry

Western blots were performed using the following antibodies: mouse anti CPT1A (abcam, 128568), rabbit anti CPT1B (abclonal, A6796), rabbit anti CPT1C (LsBio, LS-C167010), rabbit and mouse anti beta-actin (Abcam). To prepare samples for immunohistochemical analysis, Mouse brains from U87 transplant experiments were perfused using 4% paraformaldehyde (PFA) and incubated overnight in PFA at 4°C for 24 hours. Tissue was washed with PBS and incubated in 20% sucrose at 4°C for a minimum of 24 hours in preparation for sectioning on a cryostat. Sections (20 μM thick) were post-fixed for 15 minutes with cold 4% paraformaldehyde followed by 3x washes with TBS prior to performing immunohistochemistry for CPT1A.

Seahorse Respirometry Methods

All respirometry studies were conducted in a Seahorse XFe96 Analyzer. All experiments were conducted at 37°C, and at pH 7.4 (intact cells) or 7.2 (permeabilized cells). On the day of the assay, glioblastoma cells were acutely spun onto Seahorse XF96 plates (600g for 5 min) coated with Cell-Tak (Corning C354240) according to manufacturer's instructions at $4.3x10^4$ cells/well. Respiratory parameters were calculated according to standard protocols[66], and all rates were corrected for non-mitochondrial respiration/background signal by subtracting the oxygen consumption rate insensitive to rotenone and antimycin A.

Intact Cells

Potential off-target effects of etomoxir in intact glioblastoma cells was assessed by measuring respiration in response to both 3 μM and 100 μM etomoxir[38]. Prior to conducting the assay, cell culture medium was replaced with DMEM (Sigma D5030) supplemented with 8 mM glucose, 2 mM pyruvate, 2 mM glutamine and 5 mM HEPES. Respiration was measured in the basal state as well as in response to 2 μM oligomycin, FCCP (two sequential pulses of 800 nM), and 0.2 μM rotenone with 1 μM antimycin A. Etomoxir (3 μM or 100 μM) was added to the assay medium 30 min prior to measurements.

Permeabilized Cells

The plasma membrane of cells was selectively permeabilized with recombinant, mutant perfringolysin O[67] and experiments were conducted as previously described[38]. Immediately prior to the assay, cell culture medium was replaced with MAS buffer containing 3 nM rPFO, 40 μM palmitoyl CoA, 1 mM malate, 0.5 mM carnitine, and 4 mM ADP. Maximal CPT-1-driven respiration rates are given as the rate stimulated by 2 μM FCCP corrected for background with 0.2 μM rotenone with 1 μM antimycin A.

Acute etomoxir treatment and fatty acid and ketone supplementation

Dissociated cultures were plated at a density of 50k cells/ml in triplicate in gliomasphere defined media containing 25 mM glucose unless otherwise indicated. Cells were incubated for 24 hours after which point 100 μM etomoxir was added to each sample and again on day 4. [(+)-Etomoxir sodium salt hydrate, Sigma Aldrich, #E1905]. For FA and ketone supplementation, 4,000 cells were plated per well (96-well plates) and incubated for 24 hours after which either FAs or ketones were added to yield the following final concentrations of each. For FA: 25-200 μM

palmitate (Sigma Aldrich, #P0500) bound to fatty-acid free BSA (5g/50mL in 10% PBS) (Sigma Aldrich, #A1595) and 500 μM carnitine (Sigma Aldrich, # C0283). For 3-OHB (Sigma Aldrich, #166898): final concentrations were 1.25-10 mM. Blood plasma concentrations of these substrates in healthy adults range from 111-260 μM palmitate and 67 μM carnitine[68, 69, 70]. Cells were allowed to grow for the indicated period of time prior to analysis using the Dojindo Cell Counting Kit 8 (#CK04-20) according to manufacturer instructions.

Cell growth analysis

Single-cell suspensions were made from bulk cultures of the U87 and primary glioma cell lines and counted using a Countess automated cell counter. Cells were plated at 50k cells/mL in 6-well plates and grown as gliomaspheres in control or experimental conditions. For ETOM experiments, cells were treated 24 hours after initial plating and treatment was re-administered on Day 4. After 7 days the gliomaspheres in each well were fully dissociated and re-counted to assess changes in cell number during treatment. This analysis of cell number examines both cell survival and proliferation in response to treatment.

Proliferation analysis with bromodeoxyuridine (BrdU)

Single cell suspensions were plated as a monolayer on laminin-coated glass coverslips (Sigma, L2020) in 24-well plates followed by a 4 day ETOM treatment. Two BrdU pulses were given 2 hours apart and cells were fixed for 15 minutes with 4% paraformaldehyde. Coverslips were washed with PBS and immunocytochemistry was performed to assess the % of BrdU-positive cells by visual microscopic cell counts.

Annexin V/PI FACS Analysis

Single cell samples were treated with 100uM ETOM for 4 days after which spheres were re-dissociated with 200 µl accumax, centrifuged, and washed 1x with PBS. Annexin V/propidium iodide (PI) staining was carried out according to manufacturer protocol using the Annexin V APC flow cytometry kit (Thermo Fisher) while including a 1µl/ml final concentration of PI. Samples were gently mixed and incubated with Annexin V/PI binding buffer and incubated for 15 minutes at room temperature protected from light. Samples were kept on ice and analyzed within 1 hour by flow cytometry.

Reactive Oxygen Species Analysis

Mitochondrial superoxide and total intracellular ROS levels were assessed according to manufacturer instructions following a 3 hour incubation with ETOM (100 µM) by FACS analysis. Mitochondrial ROS was detected using MitoSOX™ Red Mitochondrial Superoxide Indicator (Thermo Fisher, M36008). Total intracellular ROS was measured using CellROX™ Deep Red Reagent, for oxidative stress detection (Thermo Fisher, C10422).

LC-MS with fully labeled ^{13}C palmitate

Gliomaspheres were dissociated into single cells with Accumax™ and 200k cells were cultured for 48 hours in 2.5 mM glucose media in triplicate for each sample. Cells were then rinsed with PBS and re-plated in 2.5 mM glucose media, either unlabeled or containing 200 µM fully-labeled ^{13}C-palmitic acid for an additional 48 hours. Cells were then centrifuged and rinsed with 1ml ice-cold 150 mM ammonium acetate (pH 7.3). Centrifugation was performed again and 1ml of ice-cold 80% methanol was added. Cells were transferred to an Eppendorf tube, and 10 nmol

norvaline (Sigma-Aldrich, N7502) was added to each sample. Samples were centrifuged for 5 min. at top speed and the supernatant was transferred into a glass vial. Samples were resuspended in 200 µl cold 80% methanol, followed again by centrifugation, after which the supernatant was added to the glass vial. Samples were dried in an EZ-2Elite evaporator. The remaining pellet was resuspended in RIPA buffer and a Bradford assay was performed to quantify protein levels for sample normalization. Dried metabolites were resuspended in 50% ACN and 5 µl loaded onto a Luna 3 µm NH2 100 A (150 × 2.0 mm) column (Phenomenex). The chromatographic separation was performed on an UltiMate 3000 RSLC (Thermo Scientific) with mobile phases A (5 mM NH4AcO pH 9.9) and B (ACN) and a flow rate of 200 µl/min. The gradient from 15% A to 95% A over 18 min. was followed by 9 min. isocratic flow at 95% A and re-equilibration. Metabolite detection was achieved with a Thermo Scientific Q Exactive mass spectrometer run in polarity switching mode (+3.5 kV/− 3.5 kV). TraceFinder 4.1 (Thermo Scientific) was used to quantify the area under the curve for metabolites by using accurate mass measurements (< 3 ppm) and the retention time of purchased reference standards. Relative amounts of metabolites were calculated by summing up all isotopologues of a given metabolite and normalized to cell number. Correction for naturally occurring ^{13}C as well as calculation of fractional contributions and clustering analyses were done in R.

Statistical Analysis

Statistical analysis was performed using either Microsoft Excel or GraphPad Prism software. The statistical significance of comparative samples was determined using an ANOVA model and two-tailed Student's t tests where appropriate. All quantitative data and associated error bars represent the mean ± either the standard deviation or standard error of the mean (SEM) as

indicated for each figure. Experiments were performed in triplicate at a minimum, with 95% confidence intervals and p values calculated for relevant comparison. For all figures, p values are represented as follows: * = $p<0.05$, ** = $p<0.01$, *** = $p<0.001$.

FIGURE LEGENDS

Figure 1. U87 GBM cells oxidize fatty acids and ketone bodies to support growth. A. Relative mRNA expression of the 3 CPT1 isoforms in GBM based on analysis of the TCGA dataset from primary human GBM tumors. B. Quantification of the effects of 100 μM ETOM treatment on U87 cell growth. Culture growth was assessed following a 7 day treatment with ETOM administered twice per week. C-D. Effects of FA and ketone supplementation under variable concentrations of glucose following a 7 day growth period in U87 cells. Error bars denote +/- SD. (* = $p<0.05$)

Figure 2. U87 GBM cells oxidize fatty acids to generate TCA cycle intermediates and currency metabolites. A-B. Effects of ETOM and CPT1A knockdown in U87 cells on fractional contribution (the percent of labeled carbons for each metabolite) and relative amounts of relevant TCA cycle intermediates and currency metabolites using ^{13}C-palmitate LC-MS analysis. Glucose concentration = 2.5 mM) Error bars = +/- SD. (*=$p<0.05$, **=$p<0.01$, ***=$p<0.001$).

Figure 3. The unrestricted ketogenic diet causes ketosis in mice transplanted with U87 cells. A. Western blot of fluc-GFP expressing U87 cells infected with either shCNTL or shCPT1A lentivirus. Quantification of 7 day growth in U87 shCNTL and U87 shCPT1A (Error bars = +/- SD). B. Basic schematic of the experimental design for the U87 shCPT1A ketogenic diet xenotransplant experiment. Cells were injected on Day 0. Mice were kept on standard chow for 4

days to allow appropriate recovery, after which half of each group was placed on the ketogenic diet. On Day 8, weekly bioluminescent imaging was initiated. On Day 21 mouse weight, blood glucose and ketone measurements were taken. C-E. Assessment of mouse weight, blood glucose, and blood ketone levels on Day 21. Error bars denote +/- SEM.

Figure 4. The ketogenic diet increases U87 tumor growth but this is overcome by CPT1A knockdown. A. Evaluation of tumor growth based on percent increase in total flux [p/s] from Week 1 measurements. Tumor growth was quantified for each individual animal and then averaged by group (Error Bars = +/- SD). B. Assessment of mouse survival over the course of the experiment. Survival was tracked for individual animals until either death or progression to a moribund state. C. Immunohistochemistry of CPT1A in sectioned tissue following brain perfusion. Tissue was sectioned at a thickness of 20 μM.

Figure 5. Primary GBM cells oxidize fatty acids and ketone bodies to support growth. A. Relative CPT1 isoform expression (mRNA) based on our microarray dataset from 67 primary gliomasphere cell lines and relative protein expression (Western blot) of CPT1 isoforms across a panel of gliomasphere cell lines. B. Western blot showing expression of CPT1A and CPT1C relative to beta-actin for the 4 lines used for Seahorse analysis. Quantification of maximal CPT1-driven respiration in lysed cells treated with palmitoyl-CoA using Seahorse analysis. C. Quantification of basal respiration (OCR) in cell lines incubated with either 0 μM, 3 μM, or 100 μM ETOM to test for potential off-target effects using Seahorse. D. Seahorse analysis to assess both endogenous and exogenous FAO. Endogenous oxidation was measured by adding 100 μM ETOM (indicated by arrow). Exogenous oxidation was measured by adding palmitic acid (FA

arrow) followed by 100uM ETOM (ETOM arrow). E-F. Effects of FA and ketone supplementation in a primary GBM cell line (HK157) under variable concentrations of glucose following a 7 day growth period. Error bars denote +/- SD.

Figure 6. Etomoxir inhibits primary GBM cell proliferation and promotes cell death while increasing mitochondrial ROS levels. A. Quantification of the effects of 7 day 100 μM ETOM treatment (administered twice per week) across a panel of primary GBM cell lines and two non-GBM controls (adult mouse-derived neurospheres and human fetal-derived neurospheres). Cell growth was calculated based on actual cell counts. Error bars = +/- SEM. Cultures that are EGFR amplified, EGFR ampified + EGFRviii mutant, IDH1 mutant, and PTEN deficient are indicated. B. Assessment of actively dividing cells by Brdu immunocytochemisty in two primary GBM lines grown for 4 days in the presence of 100 μM ETOM. C. FACS analysis of cell death using dual Annexin V/PI staining in HK157 cells following 4 day treatment with 100 μM ETOM. D. Evaluation of total ROS levels (CellROX Deep Red) and mitochondrial superoxide levels (with MitoSOX Red Reagent) by flow cytometry. Left: histogram showing actual fluorescent readout of one cell line. Right: Graph quantifying mean fluorescent intensities for each line. E. 7 day growth assessment (cell counts) with 100 μM ETOM, 50 mM palmitate (FA), and 1.25 mM 3-OHB in 2.5 mM glucose. All other experiments were performed in 25 mM glucose. Error bars = +/- SD.

Figure 7. GBM cells oxidize FAs to generate acetyl-CoA for use within the TCA cycle. A-B. LC-MS analysis of ^{13}C-palmitic acid fractional contribution following treatment with 100 μM ETOM. A. Heat map showing effects of ETOM on fractional contribution across metabolites. B. Quantification of the effects of ETOM on intracellular carbon labeling of acetyl-CoA, palmitic

acid, and other relevant metabolites associated with the TCA cycle. C. Effects of ETOM on relative amounts of relevant metabolites as in B. ETOM concentration used: 100 μM. Error bars = +/- SD. (* = $p<0.05$, ** = $p<0.01$, *** = $p<0.001$).

Figure 8. IDH1 mutant GBM cells express higher levels of CPT1A and utilize fatty acids to produce 2-HG. A. mRNA expression of CPT1 isoforms in IDH1 mutant and wildtype primary GBM cultures based on analysis of microarray data as in Figure 5A. B. Protein expression (Western blot) of CPT1A and CPT1C across a panel of IDH wildtype and IDH1 mutant lines. C-D. Analysis of the effects of ETOM (100 μM) in an IDH1 mutant cell line on fractional contribution and relative amounts of relevant metabolites using ^{13}C-palmitic acid LC-MS. Error bars = +/- SD. (* = $p<0.05$, ** = $p<0.01$, *** = $p<0.001$).

Supplementary Figure 1. CRISPR/Cas9 model validates the effects of the ketogenic diet and shCPT1A knockdown on U87 tumor growth. A. Western blot showing expression of CPT1A relative to beta-actin for cells infected with either CNTL or CPT1A CRISPR guideRNA/Cas9. B. Evaluation of tumor growth based on percent increase in total flux [p/s] from Week 1 measurements. Tumor growth was quantified for each individual animal and then averaged by group (Error Bars = +/- SD). The experimental design for these transplants can be found in Figure 3B.

Supplementary Figure 2. CPT1C knockdown inhibits U87 cell growth *in vitro* but does not affect tumor growth *in vivo*. A. Protein expression of CPT1C and growth quantification of U87 cells expressing either shCNTL or shCPT1C vectors. B-C. Representative images and

quantification of tumor growth (total flux [p/s]) in animals injected with shCNTL or shCPT1C-expressing U87 cells as in A.

Supplementary Figure 3. CPT1 inhibition with ETOM does not alter relative amounts of TCA metabolites in IDH1 mutant cells. Analysis of the effects of 100 μM ETOM on relative amounts of TCA metabolites in an IDH1 mutant line using ^{13}C-palmitic acid (LC-MS). Error bars = +/- SD. p-value = >0.5 (N.S.) for all metabolites shown.

Supplementary Table 1. GBM cells utilize fatty acids to support other metabolic pathways in addition to the TCA cycle. List of all metabolites significantly altered by ETOM (100 μM) treatment with regard to fractional contribution and relative amounts of labeled ^{13}C-palmitic acid using LC-MS analysis. Cell line: HK157. ($p<0.05$ for all metabolites listed).

Supplementary Table 2. IDH1 mutant GBM cells may utilize FAs differently than IDH wildtype. Identical analysis to that of Supplementary Table 1 showing all metabolites that are significantly altered by ETOM (100 μM) treatment in an IDH1 mutant line (HK252). The metabolites listed in Supplementary Table 1 are from analysis of an IDH wildtype line. ($p<0.05$ for all metabolites listed).

References

1. Agnihotri, S. & Zadeh, G. Metabolic reprogramming in glioblastoma: the influence of cancer metabolism on epigenetics and unanswered questions. *Neuro-oncology* **18**, 160–172 (2016).

2. Vander Heiden, M. G., Cantley, L. C. & Thompson, C. B. Understanding the Warburg effect: the metabolic requirements of cell proliferation. *Science* **324**, 1029–1033 (2009).

3. Yang, J. *et al.* Targeting PI3K in cancer: mechanisms and advances in clinical trials. *Mol. Cancer* **18**, 26 (2019).

4. Tateishi, K. *et al.* Myc-Driven Glycolysis Is a Therapeutic Target in Glioblastoma. *Clin. Cancer Res.* **22**, 4452–4465 (2016).

5. Felsberg, J. *et al.* Epidermal Growth Factor Receptor Variant III (EGFRvIII) Positivity in EGFR-Amplified Glioblastomas: Prognostic Role and Comparison between Primary and Recurrent Tumors. *Clin. Cancer Res.* **23**, 6846–6855 (2017).

6. Benitez, J. A. *et al.* PTEN regulates glioblastoma oncogenesis through chromatin-associated complexes of DAXX and histone H3.3. *Nat Commun* **8**, 15223 (2017).

7. Strickland, M. & Stoll, E. A. Metabolic Reprogramming in Glioma. *Front Cell Dev Biol* **5**, 43 (2017).

8. Tanaka, K. *et al.* Compensatory glutamine metabolism promotes glioblastoma resistance to mTOR inhibitor treatment. *J. Clin. Invest.* **125**, 1591–1602 (2015).

9. Liu, D. D. *et al.* Effects of inhibiting PI3K-Akt-mTOR pathway on lipid metabolism homeostasis in goose primary hepatocytes. *Animal* **10**, 1319–1327 (2016).

10. Woolf, E. C., Syed, N. & Scheck, A. C. Tumor Metabolism, the Ketogenic Diet and β-Hydroxybutyrate: Novel Approaches to Adjuvant Brain Tumor Therapy. *Front Mol Neurosci* **9**, 122 (2016).

11. Dang, L. *et al.* Cancer-associated IDH1 mutations produce 2-hydroxyglutarate. *Nature* **462**, 739–744 (2009).

12. Garrett, M. *et al.* Metabolic characterization of isocitrate dehydrogenase (IDH) mutant and IDH wildtype gliomaspheres uncovers cell type-specific vulnerabilities. *Cancer Metab* **6**, 4 (2018).
13. Molenaar, R. J., Maciejewski, J. P., Wilmink, J. W. & van Noorden, C. J. F. Wild-type and mutated IDH1/2 enzymes and therapy responses. *Oncogene* **37**, 1949–1960 (2018).
14. Núñez, F. J. *et al.* IDH1-R132H acts as a tumor suppressor in glioma via epigenetic up-regulation of the DNA damage response. *Sci Transl Med* **11**, (2019).
15. Vidali, S. *et al.* Mitochondria: The ketogenic diet--A metabolism-based therapy. *Int. J. Biochem. Cell Biol.* **63**, 55–59 (2015).
16. Maurer, G. D. *et al.* Differential utilization of ketone bodies by neurons and glioma cell lines: a rationale for ketogenic diet as experimental glioma therapy. *BMC Cancer* **11**, 315 (2011).
17. Cahill, G. F. Fuel metabolism in starvation. *Annu. Rev. Nutr.* **26**, 1–22 (2006).
18. Stafford, P. *et al.* The ketogenic diet reverses gene expression patterns and reduces reactive oxygen species levels when used as an adjuvant therapy for glioma. *Nutr Metab (Lond)* **7**, 74 (2010).
19. Rieger, J. *et al.* ERGO: a pilot study of ketogenic diet in recurrent glioblastoma. *Int. J. Oncol.* **44**, 1843–1852 (2014).
20. Zhou, W. *et al.* The calorically restricted ketogenic diet, an effective alternative therapy for malignant brain cancer. *Nutr Metab (Lond)* **4**, 5 (2007).
21. Nagarajan, A., Malvi, P. & Wajapeyee, N. Oncogene-directed alterations in cancer cell metabolism. *Trends Cancer* **2**, 365–377 (2016).

22. Guo, D. *et al.* EGFR signaling through an Akt-SREBP-1-dependent, rapamycin-resistant pathway sensitizes glioblastomas to antilipogenic therapy. *Sci Signal* **2**, ra82 (2009).

23. Yecies, J. L. *et al.* Akt stimulates hepatic SREBP1c and lipogenesis through parallel mTORC1-dependent and independent pathways. *Cell Metab.* **14**, 21–32 (2011).

24. Guo, D., Bell, E. H., Mischel, P. & Chakravarti, A. Targeting SREBP-1-driven lipid metabolism to treat cancer. *Curr. Pharm. Des.* **20**, 2619–2626 (2014).

25. Ricoult, S. J. H., Yecies, J. L., Ben-Sahra, I. & Manning, B. D. Oncogenic PI3K and K-Ras stimulate de novo lipid synthesis through mTORC1 and SREBP. *Oncogene* **35**, 1250–1260 (2016).

26. Pike, L. S., Smift, A. L., Croteau, N. J., Ferrick, D. A. & Wu, M. Inhibition of fatty acid oxidation by etomoxir impairs NADPH production and increases reactive oxygen species resulting in ATP depletion and cell death in human glioblastoma cells. *Biochim. Biophys. Acta* **1807**, 726–734 (2011).

27. Sayre, N. L. *et al.* Stimulation of astrocyte fatty acid oxidation by thyroid hormone is protective against ischemic stroke-induced damage. *J. Cereb. Blood Flow Metab.* **37**, 514–527 (2017).

28. Williams, W. M., Chang, M. C., Hayakawa, T., Grange, E. & Rapoport, S. I. In vivo incorporation from plasma of radiolabeled palmitate and arachidonate into rat brain microvessels. *Microvasc. Res.* **53**, 163–166 (1997).

29. Spector, R. Fatty acid transport through the blood-brain barrier. *J. Neurochem.* **50**, 639–643 (1988).

30. Lam, T. K. T. *et al.* Hypothalamic sensing of circulating fatty acids is required for glucose homeostasis. *Nat. Med.* **11**, 320–327 (2005).

31. Lin, H. *et al.* Fatty acid oxidation is required for the respiration and proliferation of malignant glioma cells. *Neuro-oncology* **19**, 43–54 (2017).

32. Duman, C. *et al.* Acyl-CoA-Binding Protein Drives Glioblastoma Tumorigenesis by Sustaining Fatty Acid Oxidation. *Cell Metab.* (2019). doi:10.1016/j.cmet.2019.04.004

33. Buzzai, M. *et al.* The glucose dependence of Akt-transformed cells can be reversed by pharmacologic activation of fatty acid beta-oxidation. *Oncogene* **24**, 4165–4173 (2005).

34. Silver, I. A. & Erecińska, M. Extracellular glucose concentration in mammalian brain: continuous monitoring of changes during increased neuronal activity and upon limitation in oxygen supply in normo-, hypo-, and hyperglycemic animals. *J. Neurosci.* **14**, 5068–5076 (1994).

35. Skinner, R., Trujillo, A., Ma, X. & Beierle, E. A. Ketone bodies inhibit the viability of human neuroblastoma cells. *J. Pediatr. Surg.* **44**, 212–216; discussion 216 (2009).

36. Seyfried, T. N., Sanderson, T. M., El-Abbadi, M. M., McGowan, R. & Mukherjee, P. Role of glucose and ketone bodies in the metabolic control of experimental brain cancer. *Br. J. Cancer* **89**, 1375–1382 (2003).

37. Laks, D. R. *et al.* Large-scale assessment of the gliomasphere model system. *Neuro-oncology* **18**, 1367–1378 (2016).

38. Divakaruni, A. S. *et al.* Etomoxir Inhibits Macrophage Polarization by Disrupting CoA Homeostasis. *Cell Metab.* **28**, 490-503.e7 (2018).

39. Yang, C. *et al.* Glioblastoma cells require glutamate dehydrogenase to survive impairments of glucose metabolism or Akt signaling. *Cancer Res.* **69**, 7986–7993 (2009).

40. Ye, F. *et al.* Protective properties of radio-chemoresistant glioblastoma stem cell clones are associated with metabolic adaptation to reduced glucose dependence. *PLoS ONE* **8**, e80397 (2013).

41. Marie, S. K. N. & Shinjo, S. M. O. Metabolism and brain cancer. *Clinics (Sao Paulo)* **66 Suppl 1**, 33–43 (2011).

42. Salzillo, T. C. *et al.* Interrogating Metabolism in Brain Cancer. *Magn Reson Imaging Clin N Am* **24**, 687–703 (2016).

43. Seyfried, T. N. *et al.* Metabolic management of brain cancer. *Biochim. Biophys. Acta* **1807**, 577–594 (2011).

44. Weber, D. D., Aminazdeh-Gohari, S. & Kofler, B. Ketogenic diet in cancer therapy. *Aging (Albany NY)* **10**, 164–165 (2018).

45. Zhang, Y., Xu, J., Zhang, K., Yang, W. & Li, B. The Anticonvulsant Effects of Ketogenic Diet on Epileptic Seizures and Potential Mechanisms. *Curr Neuropharmacol* **16**, 66–70 (2018).

46. Youngson, N. A., Morris, M. J. & Ballard, J. W. O. The mechanisms mediating the antiepileptic effects of the ketogenic diet, and potential opportunities for improvement with metabolism-altering drugs. *Seizure* **52**, 15–19 (2017).

47. Simeone, T. A., Matthews, S. A., Samson, K. K. & Simeone, K. A. Regulation of brain PPARgamma2 contributes to ketogenic diet anti-seizure efficacy. *Exp. Neurol.* **287**, 54–64 (2017).

48. De Feyter, H. M. *et al.* A ketogenic diet increases transport and oxidation of ketone bodies in RG2 and 9L gliomas without affecting tumor growth. *Neuro-oncology* **18**, 1079–1087 (2016).

49. Lussier, D. M. *et al.* Enhanced immunity in a mouse model of malignant glioma is mediated by a therapeutic ketogenic diet. *BMC Cancer* **16**, 310 (2016).

50. Meidenbauer, J. J., Ta, N. & Seyfried, T. N. Influence of a ketogenic diet, fish-oil, and calorie restriction on plasma metabolites and lipids in C57BL/6J mice. *Nutr Metab (Lond)* **11**, 23 (2014).

51. Jiang, Y.-S. & Wang, F.-R. Caloric restriction reduces edema and prolongs survival in a mouse glioma model. *J. Neurooncol.* **114**, 25–32 (2013).

52. Mukherjee, P., El-Abbadi, M. M., Kasperzyk, J. L., Ranes, M. K. & Seyfried, T. N. Dietary restriction reduces angiogenesis and growth in an orthotopic mouse brain tumour model. *Br. J. Cancer* **86**, 1615–1621 (2002).

53. Schwartz, K. *et al.* Treatment of glioma patients with ketogenic diets: report of two cases treated with an IRB-approved energy-restricted ketogenic diet protocol and review of the literature. *Cancer Metab* **3**, 3 (2015).

54. Zuccoli, G. *et al.* Metabolic management of glioblastoma multiforme using standard therapy together with a restricted ketogenic diet: Case Report. *Nutr Metab (Lond)* **7**, 33 (2010).

55. Nebeling, L. C., Miraldi, F., Shurin, S. B. & Lerner, E. Effects of a ketogenic diet on tumor metabolism and nutritional status in pediatric oncology patients: two case reports. *J Am Coll Nutr* **14**, 202–208 (1995).

56. Cirillo, A. *et al.* High grade glioblastoma is associated with aberrant expression of ZFP57, a protein involved in gene imprinting, and of CPT1A and CPT1C that regulate fatty acid metabolism. *Cancer Biol. Ther.* **15**, 735–741 (2014).

57. Elstrom, R. L. *et al.* Akt stimulates aerobic glycolysis in cancer cells. *Cancer Res.* **64**, 3892–3899 (2004).

58. Maroon, J. C., Seyfried, T. N., Donohue, J. P. & Bost, J. The role of metabolic therapy in treating glioblastoma multiforme. *Surg Neurol Int* **6**, 61 (2015).

59. Schönfeld, P. & Reiser, G. Why does brain metabolism not favor burning of fatty acids to provide energy? Reflections on disadvantages of the use of free fatty acids as fuel for brain. *J. Cereb. Blood Flow Metab.* **33**, 1493–1499 (2013).

60. Srivastava, N. K., Pradhan, S., Gowda, G. A. N. & Kumar, R. In vitro, high-resolution 1H and 31P NMR based analysis of the lipid components in the tissue, serum, and CSF of the patients with primary brain tumors: one possible diagnostic view. *NMR Biomed* **23**, 113–122 (2010).

61. Mashimo, T. *et al.* Acetate is a bioenergetic substrate for human glioblastoma and brain metastases. *Cell* **159**, 1603–1614 (2014).

62. Fraser, D. D. *et al.* Elevated polyunsaturated fatty acids in blood serum obtained from children on the ketogenic diet. *Neurology* **60**, 1026–1029 (2003).

63. Taha, A. Y., Ryan, M. A. A. & Cunnane, S. C. Despite transient ketosis, the classic high-fat ketogenic diet induces marked changes in fatty acid metabolism in rats. *Metab. Clin. Exp.* **54**, 1127–1132 (2005).

64. Cancer Genome Atlas Research Network *et al.* Comprehensive, Integrative Genomic Analysis of Diffuse Lower-Grade Gliomas. *N. Engl. J. Med.* **372**, 2481–2498 (2015).

65. Laks, D. R. *et al.* Neurosphere formation is an independent predictor of clinical outcome in malignant glioma. *Stem Cells* **27**, 980–987 (2009).

66. Divakaruni, A. S., Paradyse, A., Ferrick, D. A., Murphy, A. N. & Jastroch, M. Analysis and interpretation of microplate-based oxygen consumption and pH data. *Meth. Enzymol.* **547**, 309–354 (2014).

67. Divakaruni, A. S. *et al.* Thiazolidinediones are acute, specific inhibitors of the mitochondrial pyruvate carrier. *Proc. Natl. Acad. Sci. U.S.A.* **110**, 5422–5427 (2013).

68. Borch, L. *et al.* Normal Levels of Plasma Free Carnitine and Acylcarnitines in Follow-Up Samples from a Presymptomatic Case of Carnitine Palmitoyl Transferase 1 (CPT1) Deficiency Detected Through Newborn Screening in Denmark. *JIMD Rep* **3**, 11–15 (2012).

69. Cunnane, S. C. *et al.* Plasma and brain fatty acid profiles in mild cognitive impairment and Alzheimer's disease. *J. Alzheimers Dis.* **29**, 691–697 (2012).

70. Jensen, M. D., Haymond, M. W., Rizza, R. A., Cryer, P. E. & Miles, J. M. Influence of body fat distribution on free fatty acid metabolism in obesity. *J. Clin. Invest.* **83**, 1168–1173 (1989).

Sperry et al
Main Figures

Figure 1.

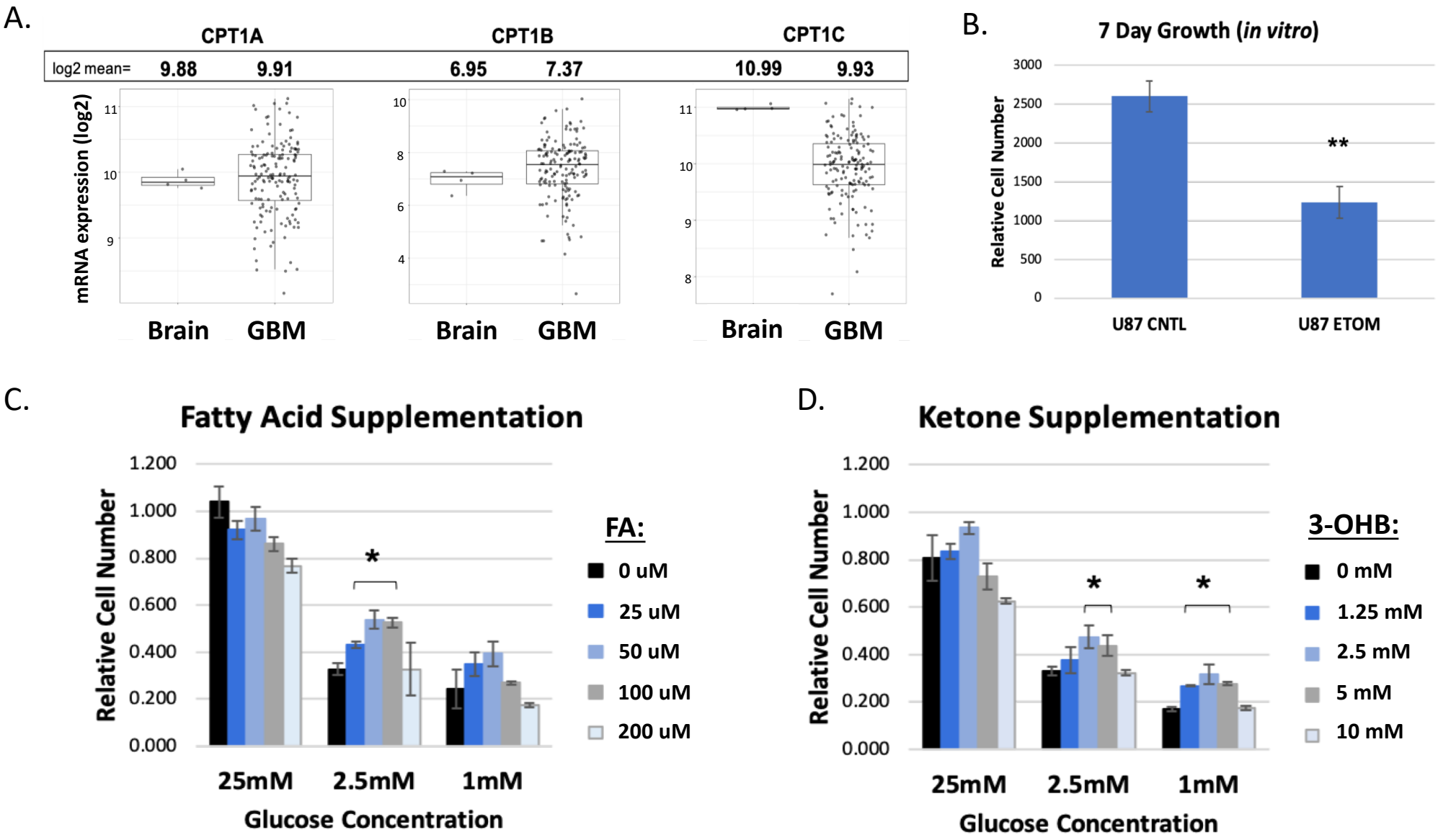
A.
CPT1A
CPT1B
CPT1C
log2 mean=
9.88
9.91
6.95
7.37
10.99
9.93
mRNA expression (log2)
Brain
GBM
B.
7 Day Growth (in vitro)
Relative Cell Number
**
U87 CNTL
U87 ETOM
C.
Fatty Acid Supplementation
Relative Cell Number
FA:
0 uM
25 uM
50 uM
100 uM
200 uM
25mM
2.5mM
1mM
Glucose Concentration
D.
Ketone Supplementation
Relative Cell Number
3-OHB:
0 mM
1.25 mM
2.5 mM
5 mM
10 mM
25mM
2.5mM
1mM
Glucose Concentration

Figure 2.

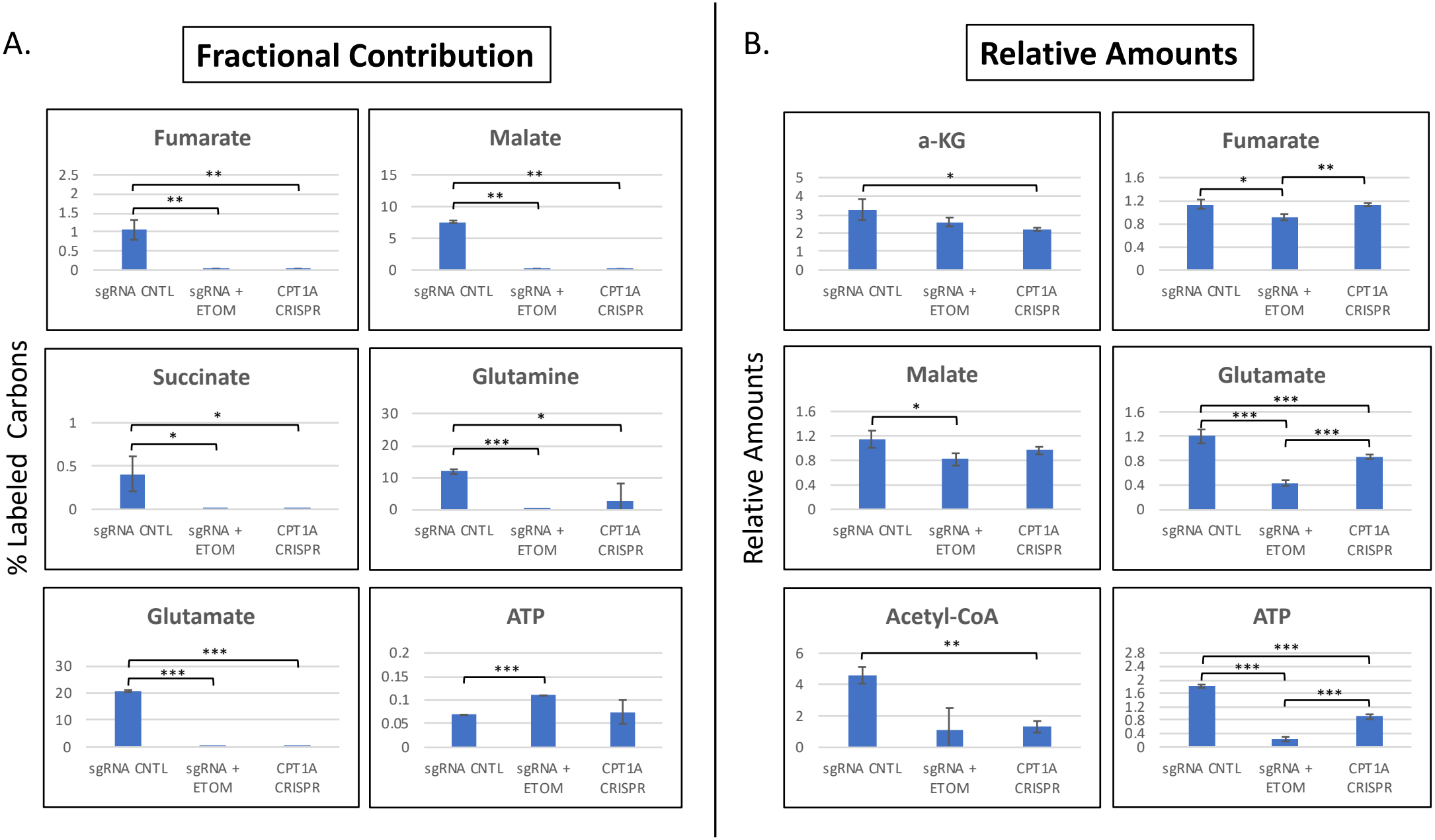
A.
Fractional Contribution
% Labeled Carbons
Fumarate
Malate
Succinate
Glutamine
Glutamate
ATP
B.
Relative Amounts
a-KG
Fumarate
Malate
Glutamate
Acetyl-CoA
ATP
sgRNA CNTL
sgRNA + ETOM
CPT1A CRISPR

Figure 3.

A.

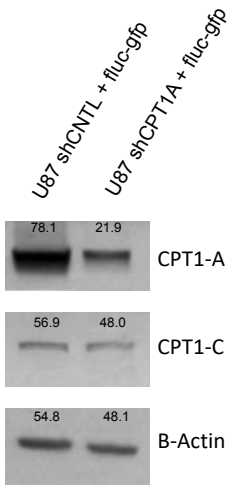

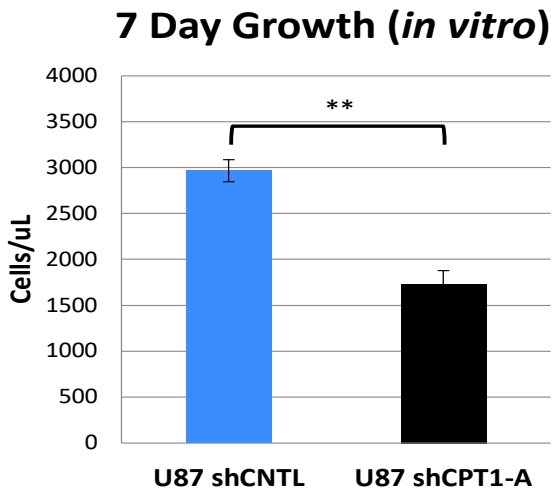

B.

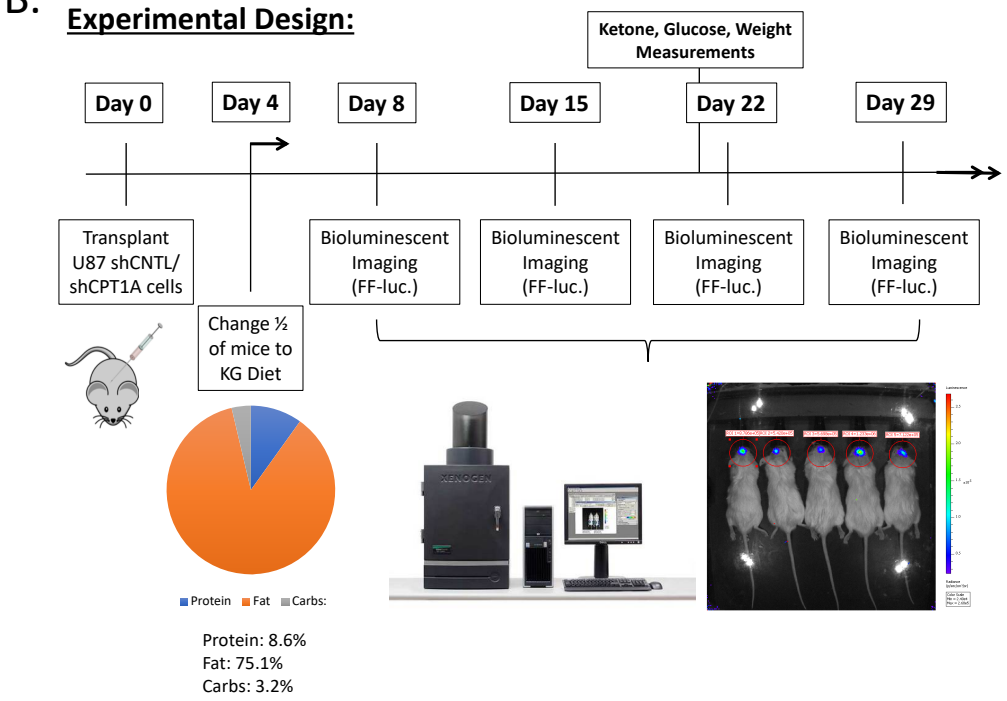

C.

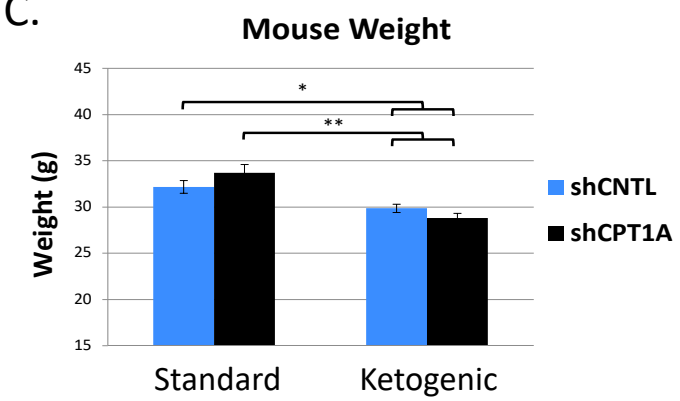

D.

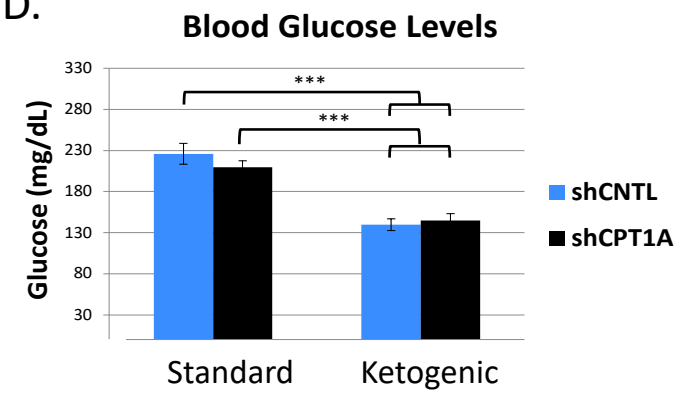

E.

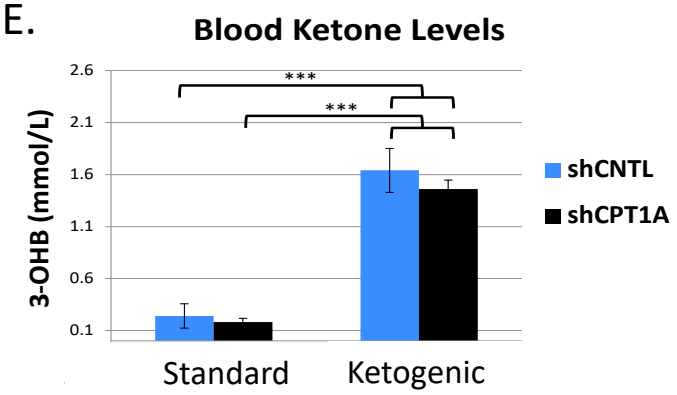

Figure 4.

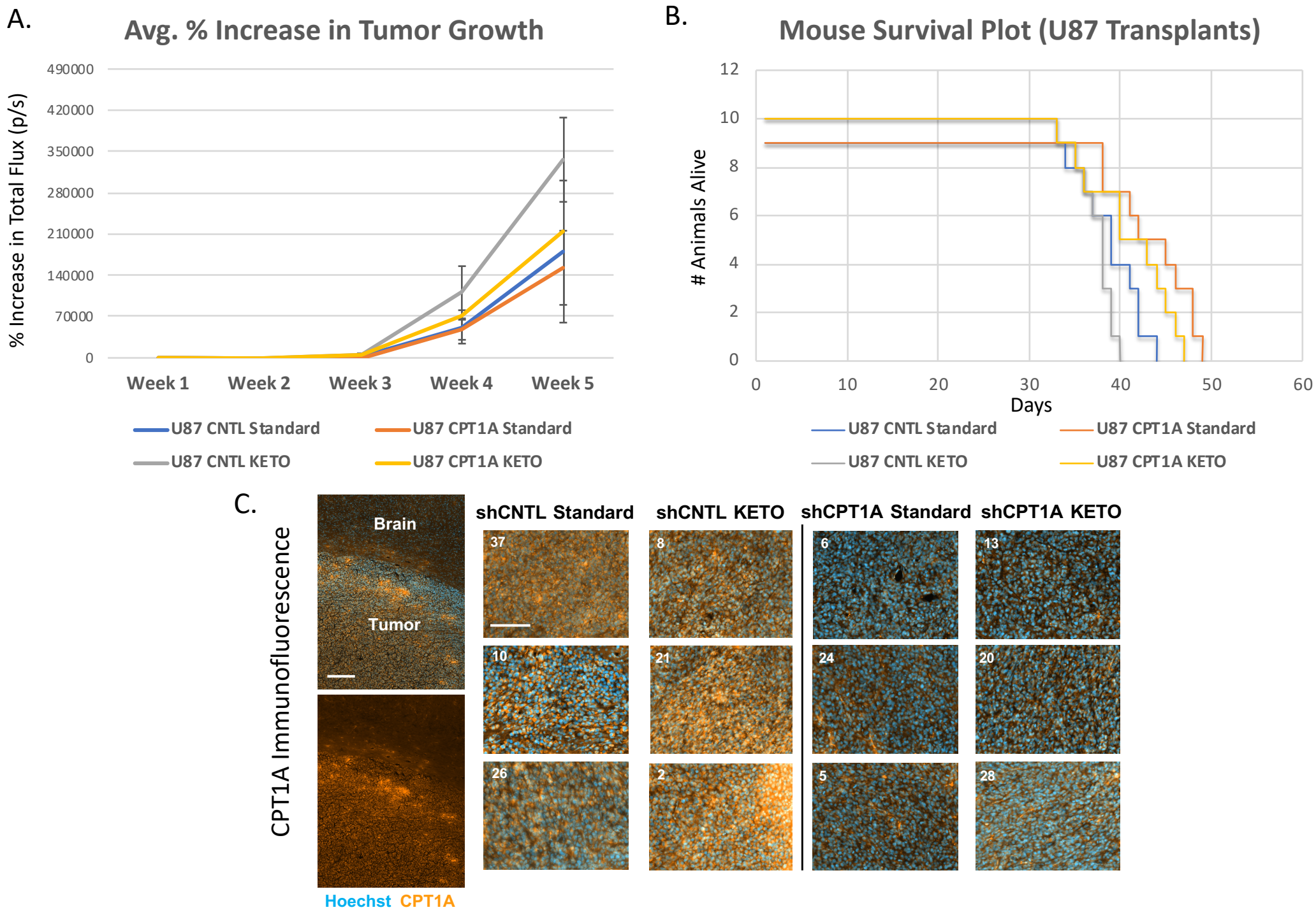
A.
Avg. % Increase in Tumor Growth
% Increase in Total Flux (p/s)
490000
420000
350000
280000
210000
140000
70000
0
Week 1
Week 2
Week 3
Week 4
Week 5
U87 CNTL Standard
U87 CPT1A Standard
U87 CNTL KETO
U87 CPT1A KETO
B.
Mouse Survival Plot (U87 Transplants)
Animals Alive
12
10
8
6
4
2
0
0
10
20
30
40
50
60
Days
U87 CNTL Standard
U87 CPT1A Standard
U87 CNTL KETO
U87 CPT1A KETO
C.
CPT1A Immunofluorescence
Brain
Tumor
Hoechst CPT1A
shCNTL Standard
shCNTL KETO
shCPT1A Standard
shCPT1A KETO
37
8
6
13
10
21
24
20
26
2
5
28

Figure 5.

A.

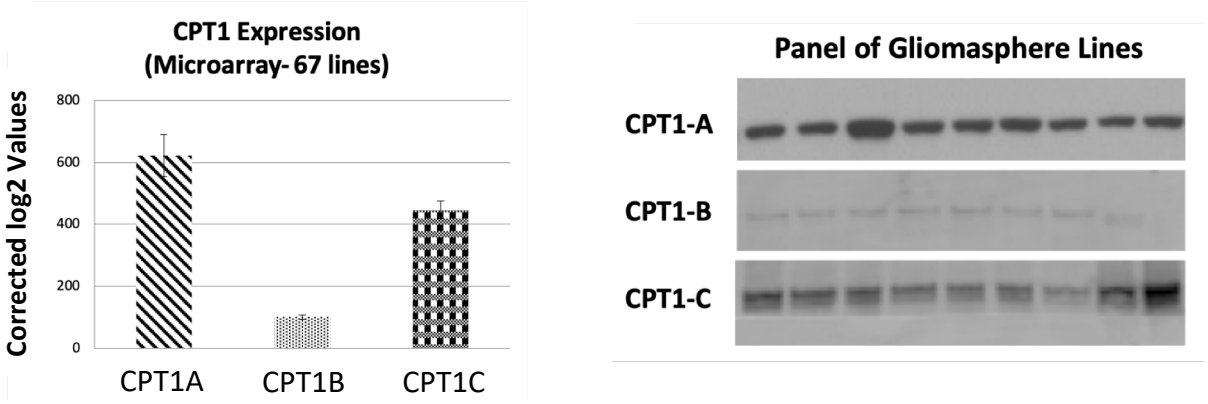

B.

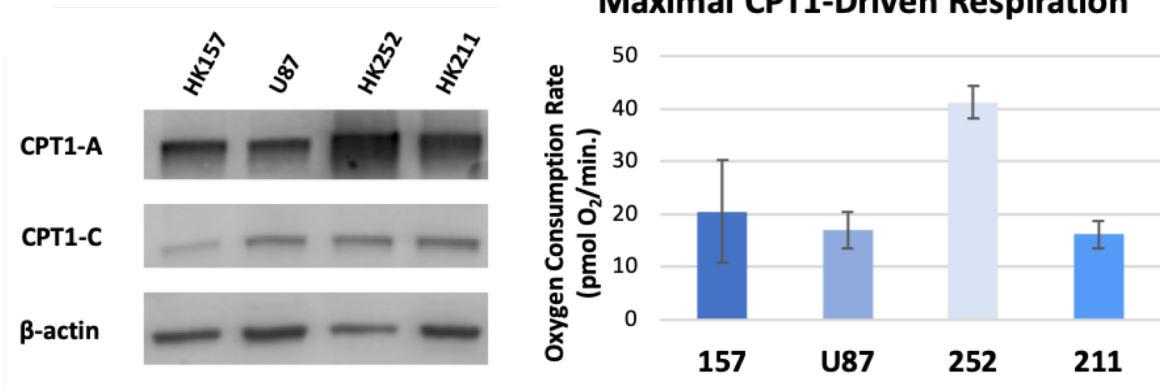

C.

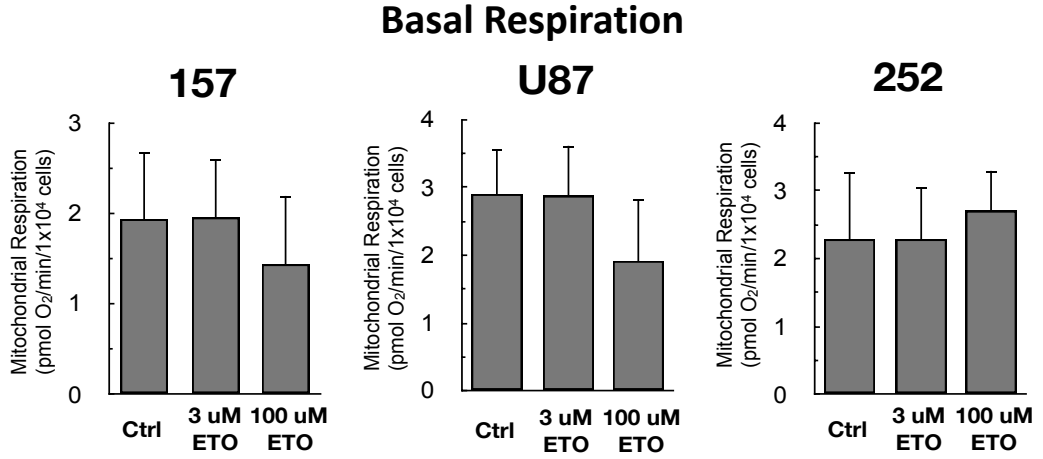

D.

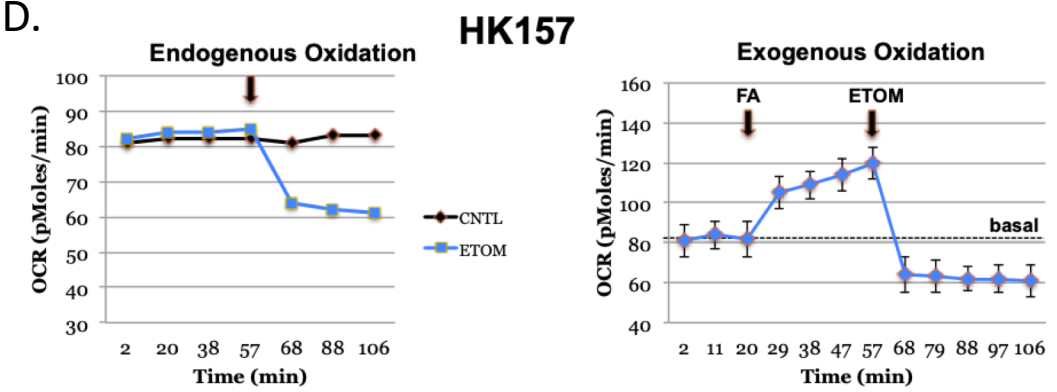

E.

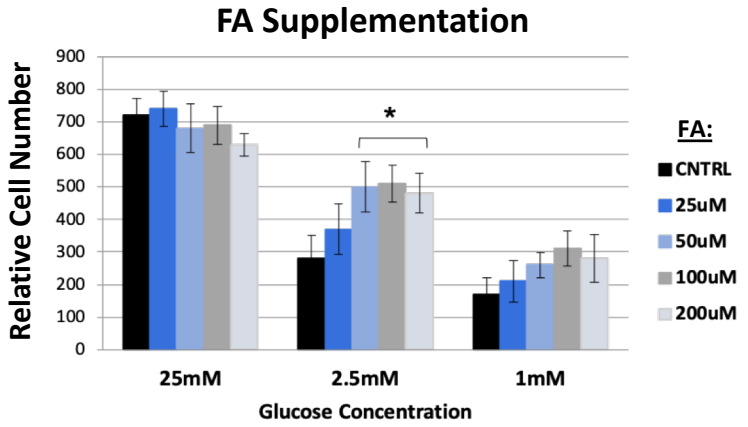

F.

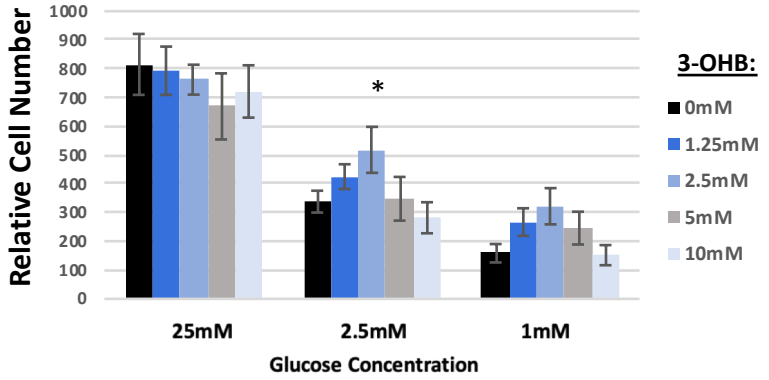

Figure 6.

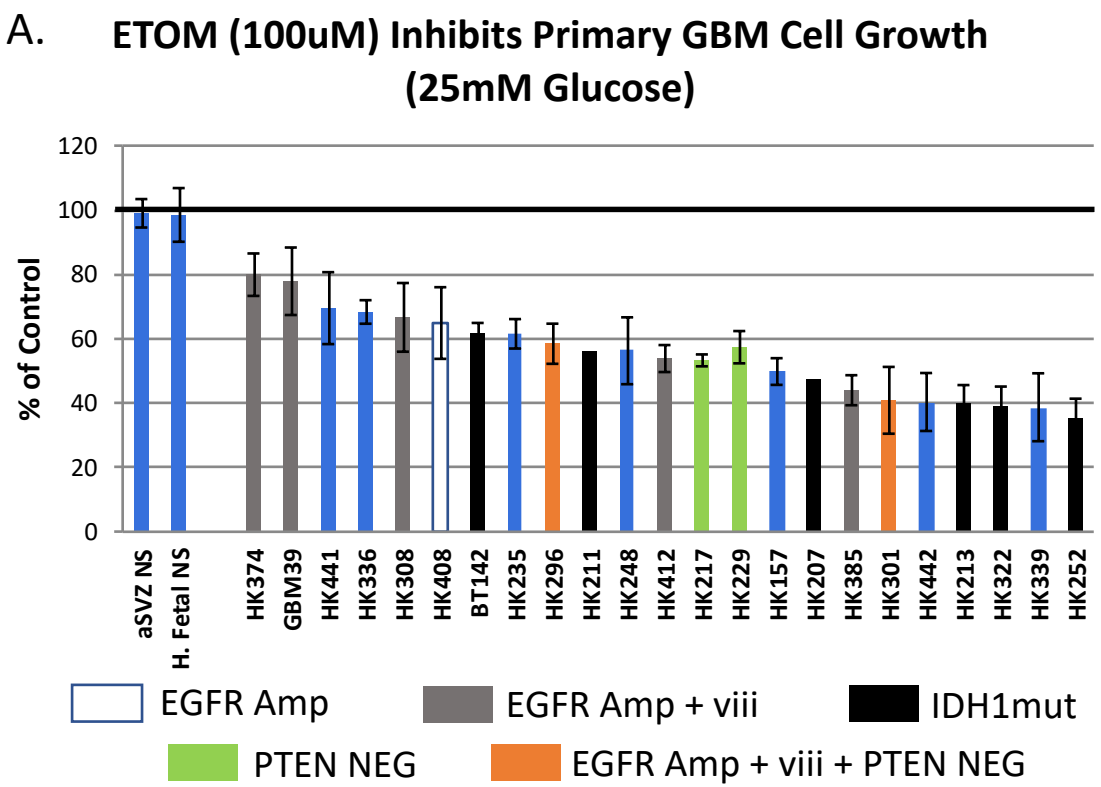
A.
ETOM (100uM) Inhibits Primary GBM Cell Growth
(25mM Glucose)
% of Control
120
100
80
60
40
20
0
aSVZ NS
H. Fetal NS
HK374
GBM39
HK441
HK336
HK308
HK408
BT142
HK235
HK296
HK211
HK248
HK412
HK217
HK229
HK157
HK207
HK385
HK301
HK442
HK213
HK322
HK339
HK252
EGFR Amp
EGFR Amp + viii
IDH1mut
PTEN NEG
EGFR Amp + viii + PTEN NEG

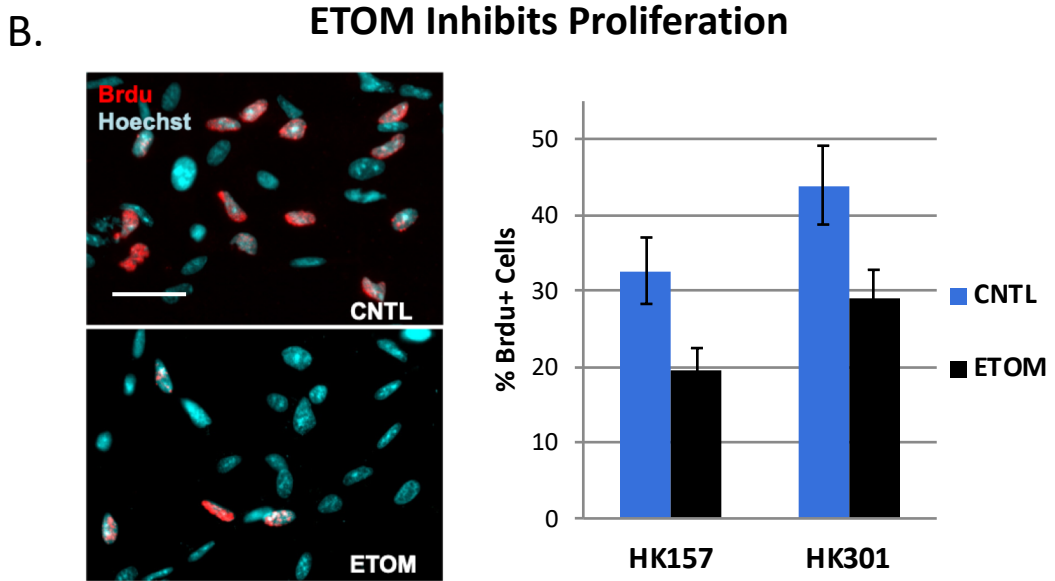
B.
ETOM Inhibits Proliferation
Brdu
Hoechst
CNTL
ETOM
% Brdu+ Cells
50
40
30
20
10
0
HK157
HK301
CNTL
ETOM

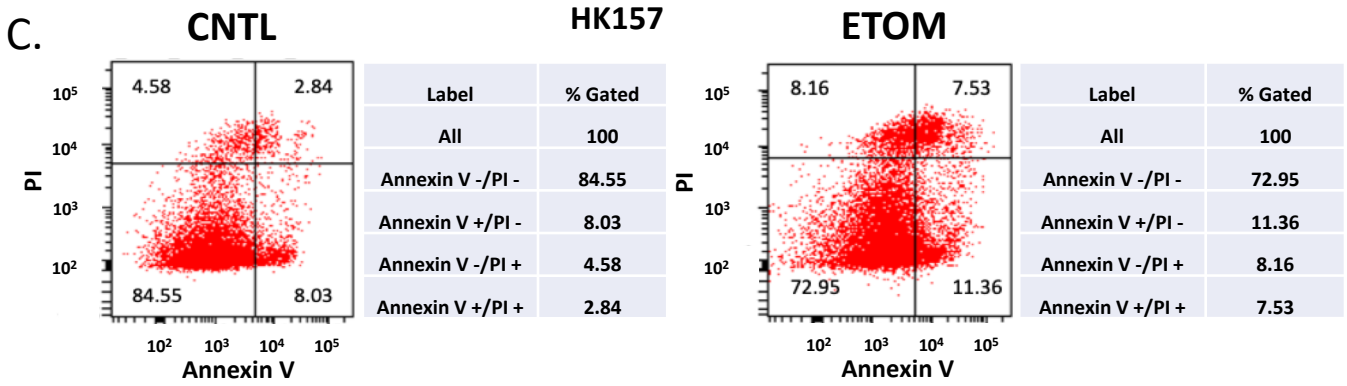
C.
CNTL
HK157
ETOM
PI
Annexin V
4.58
2.84
84.55
8.03
Label
% Gated
All
100
Annexin V -/PI -
84.55
Annexin V +/PI -
8.03
Annexin V -/PI +
4.58
Annexin V +/PI +
2.84
8.16
7.53
72.95
11.36
Label
% Gated
All
100
Annexin V -/PI -
72.95
Annexin V +/PI -
11.36
Annexin V -/PI +
8.16
Annexin V +/PI +
7.53

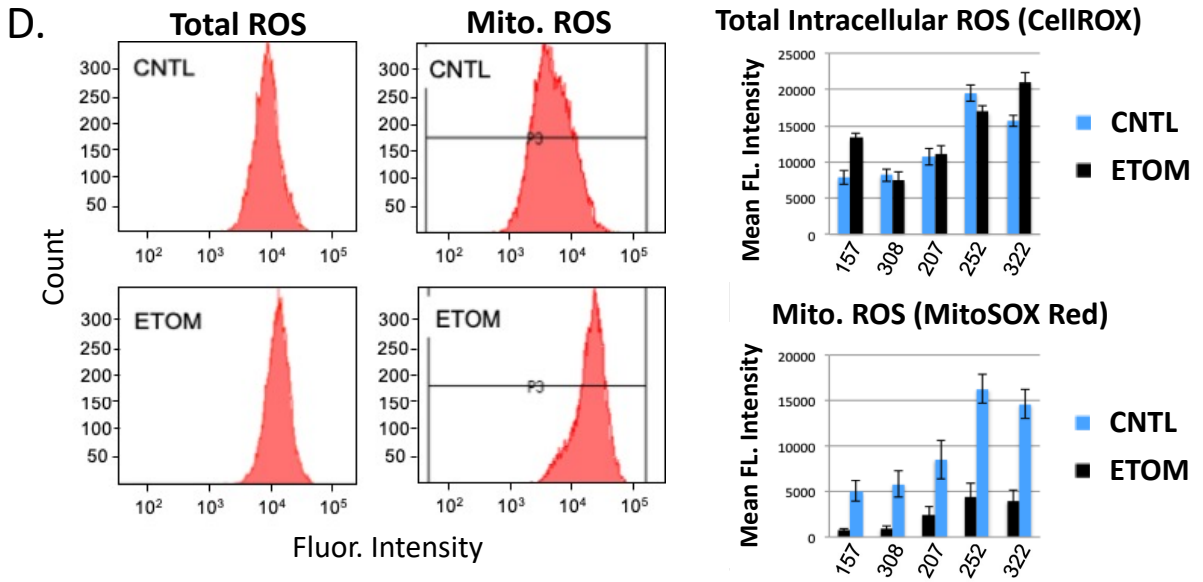
D.
Total ROS
Mito. ROS
CNTL
ETOM
Count
Fluor. Intensity
Total Intracellular ROS (CellROX)
Mean FL. Intensity
CNTL
ETOM
Mito. ROS (MitoSOX Red)
Mean FL. Intensity
CNTL
ETOM
157
308
207
252
322

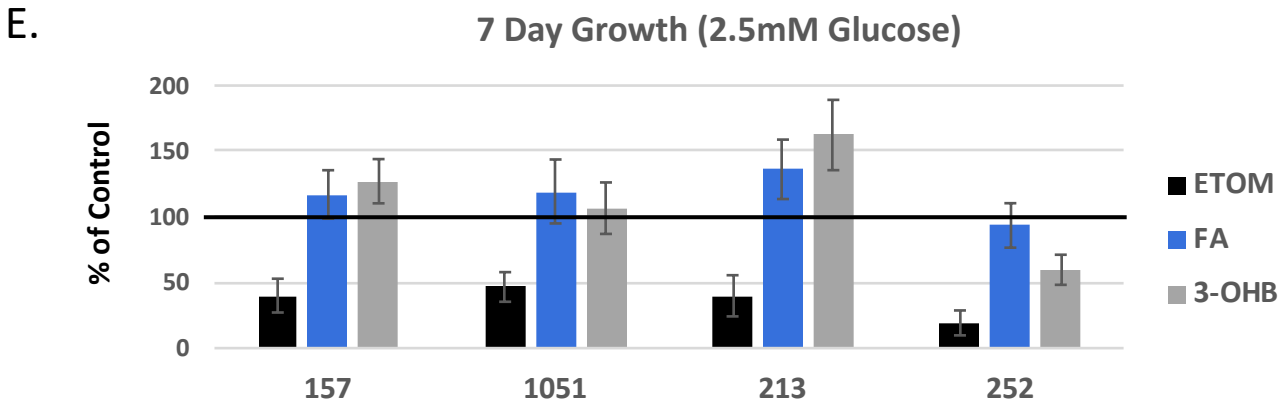
E.
7 Day Growth (2.5mM Glucose)
% of Control
200
150
100
50
0
157
1051
213
252
ETOM
FA
3-OHB

Figure 7.

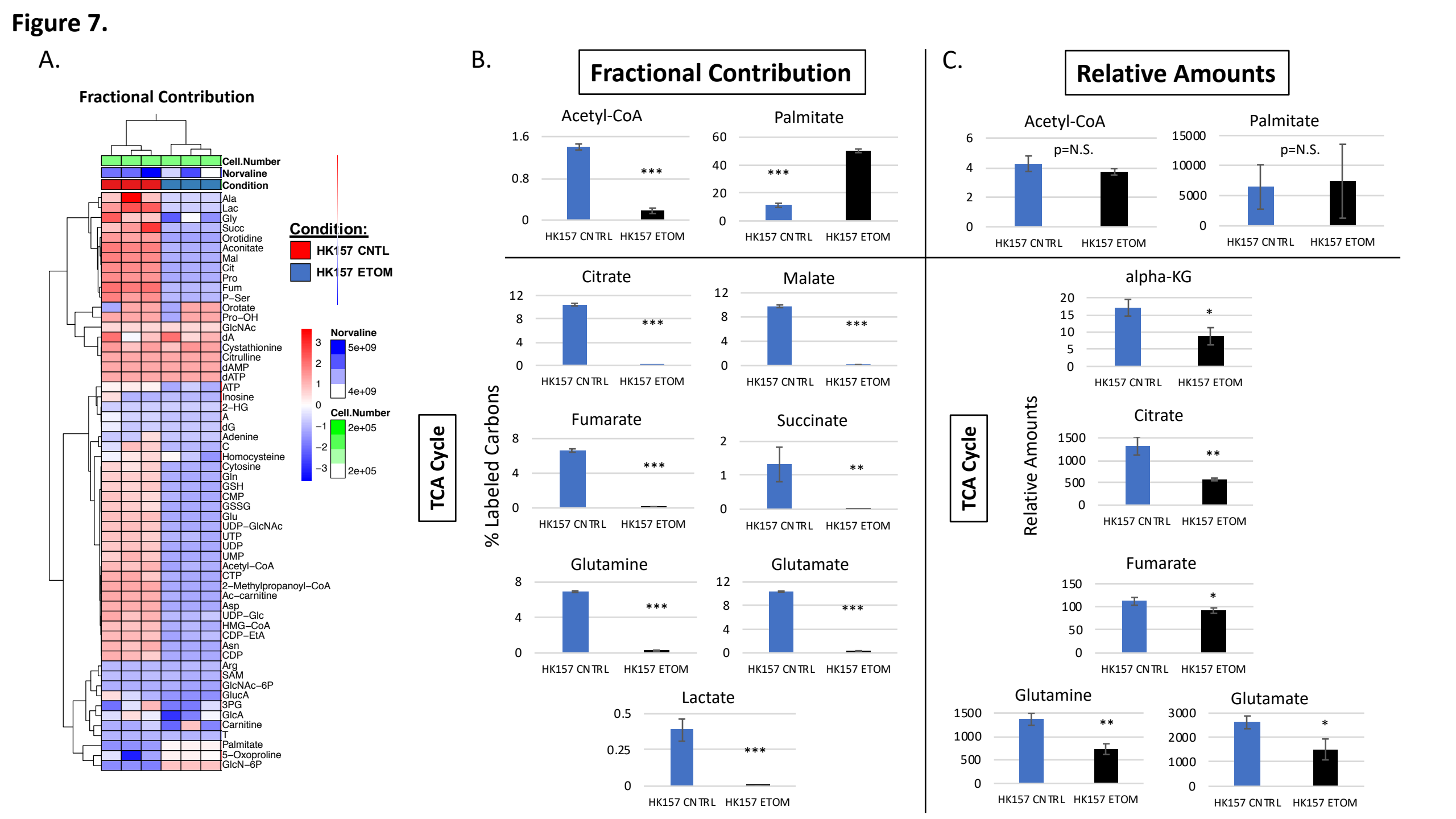
A.
Fractional Contribution
Cell.Number
Norvaline
Condition
Ala
Lac
Gly
Succ
Orotidine
Aconitate
Mal
Cit
Pro
Fum
P–Ser
Orotate
Pro–OH
GlcNAc
dA
Cystathionine
Citrulline
dAMP
dATP
ATP
Inosine
2–HG
A
dG
Adenine
C
Homocysteine
Cytosine
Gln
GSH
CMP
GSSG
Glu
UDP–GlcNAc
UTP
UDP
UMP
Acetyl–CoA
CTP
2–Methylpropanoyl–CoA
Ac–carnitine
Asp
UDP–Glc
HMG–CoA
CDP–EtA
Asn
CDP
Arg
SAM
GlcNAc–6P
GlucA
3PG
GlcA
Carnitine
T
Palmitate
5–Oxoproline
GlcN–6P
Condition:
HK157 CNTL
HK157 ETOM
Norvaline
5e+09
4e+09
Cell.Number
2e+05
2e+05
B.
Fractional Contribution
TCA Cycle
% Labeled Carbons
Acetyl-CoA
Palmitate
Citrate
Malate
Fumarate
Succinate
Glutamine
Glutamate
Lactate
HK157 CNTRL
HK157 ETOM
***
**
C.
Relative Amounts
TCA Cycle
Relative Amounts
Acetyl-CoA
p=N.S.
Palmitate
p=N.S.
alpha-KG
Citrate
Fumarate
Glutamine
Glutamate
HK157 CNTRL
HK157 ETOM
*
**

Figure 8.

A.

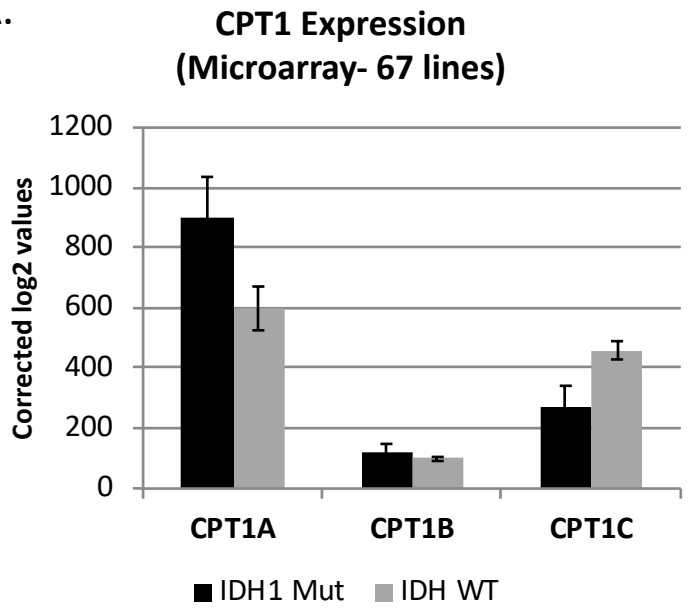

B.

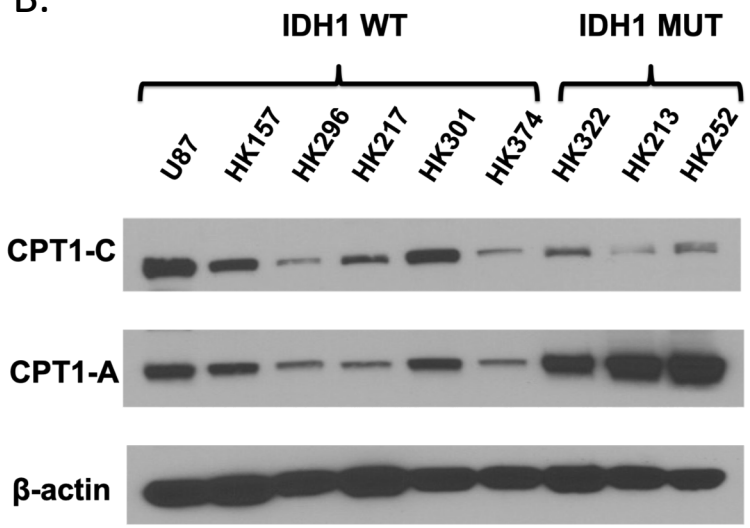

C.

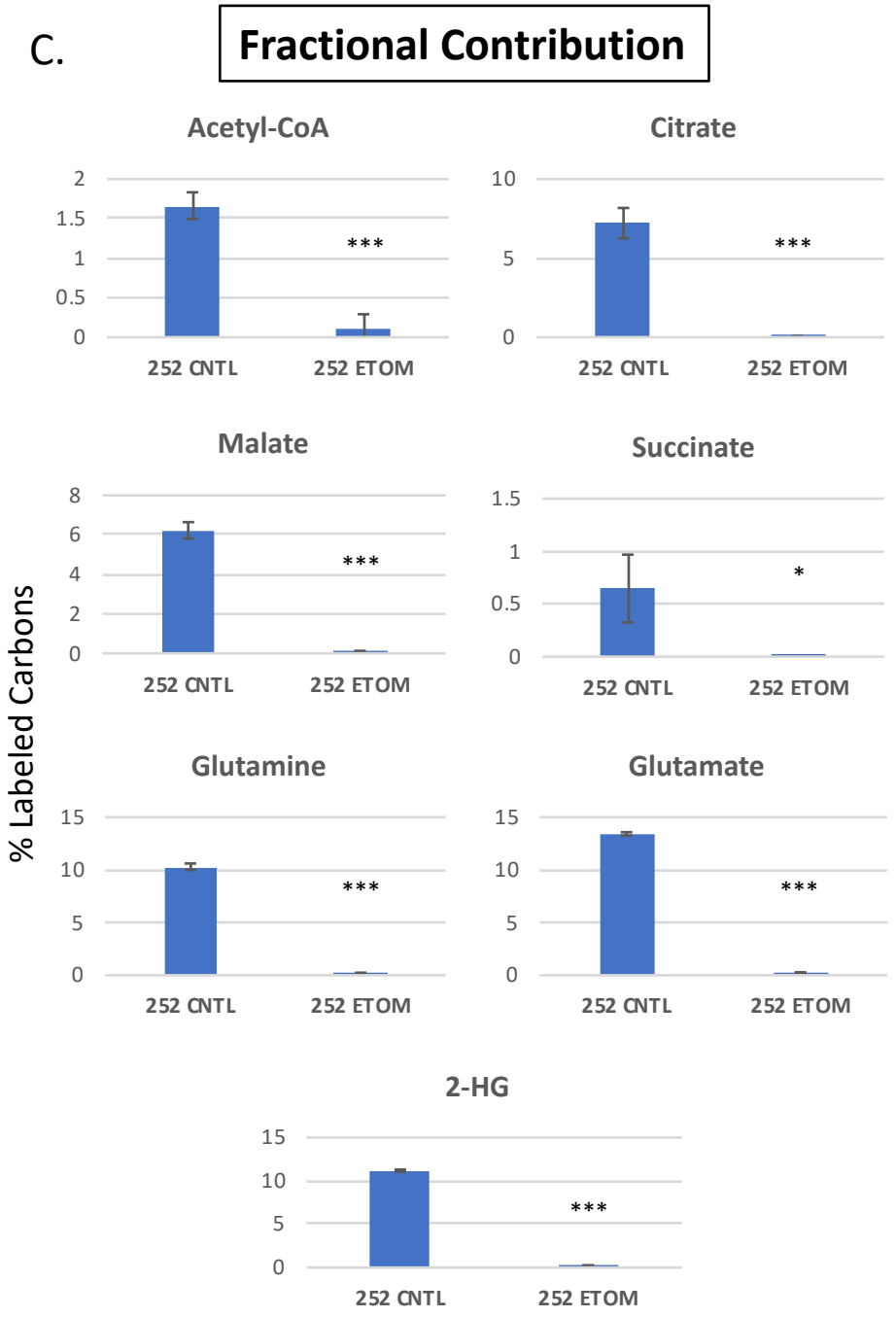

D.

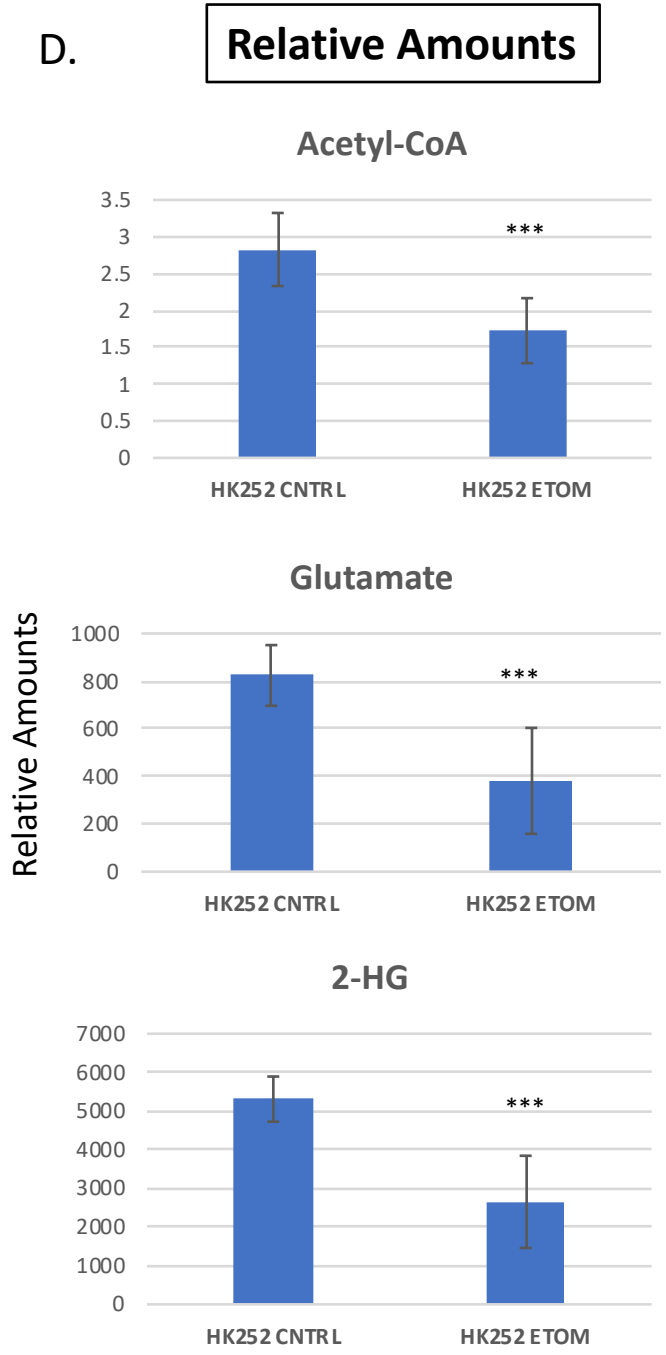

Sperry et al. Supplementary Figures and Tables

Supplementary Figure 1.

A.

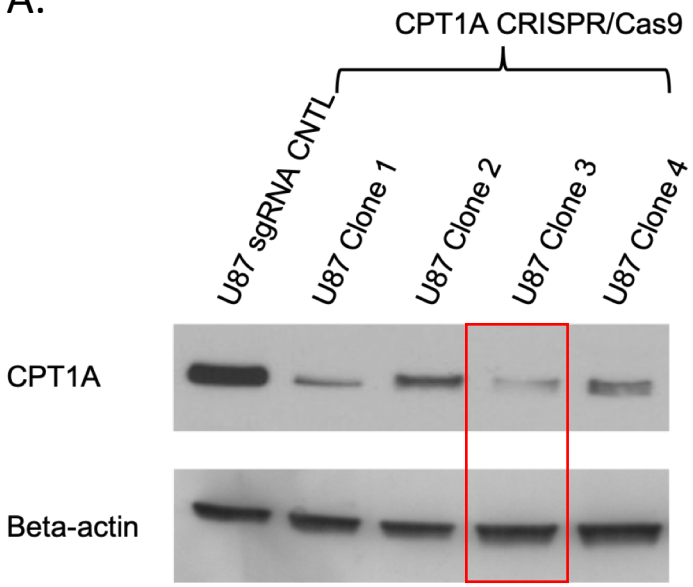

B.

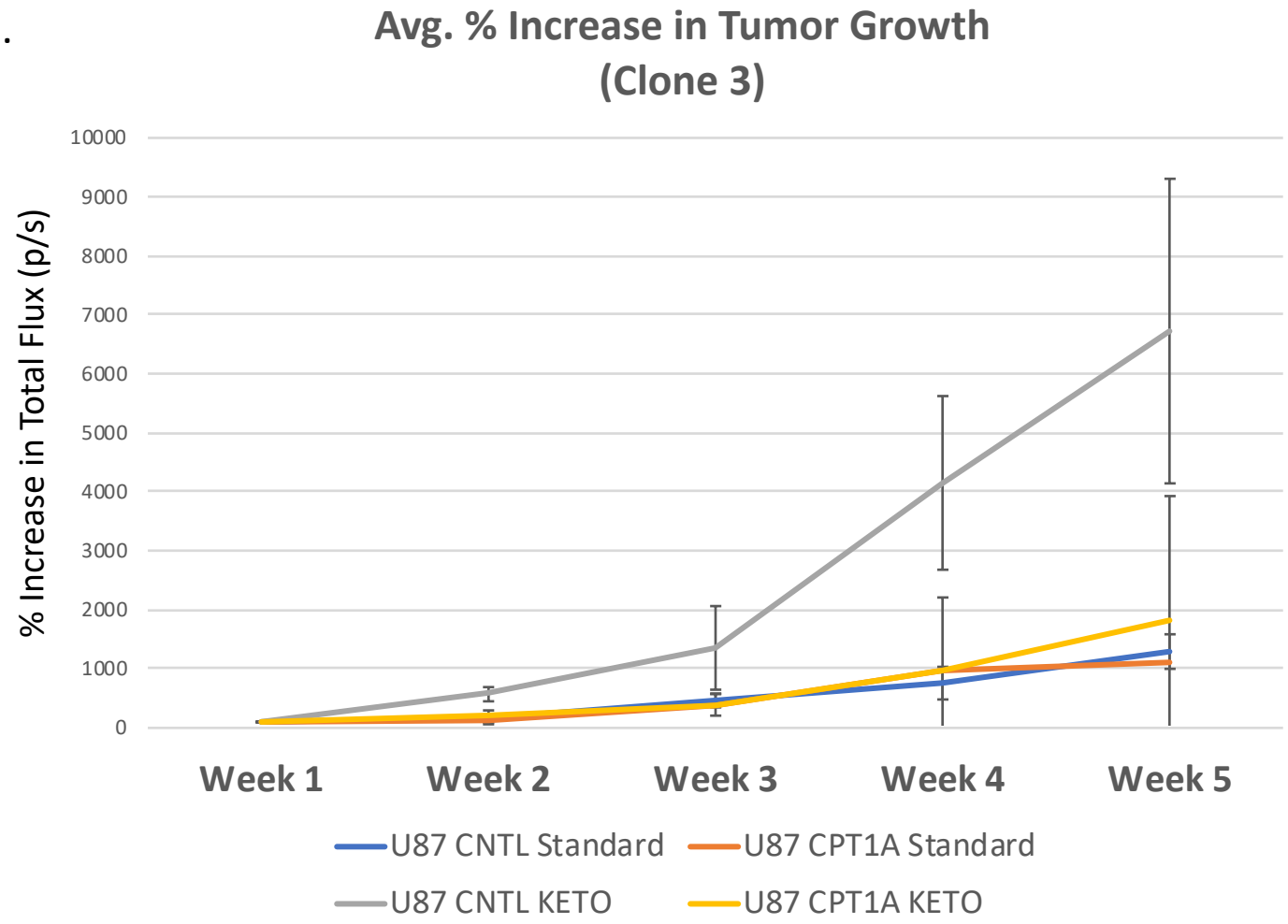

Supplementary Figure 2.

A.

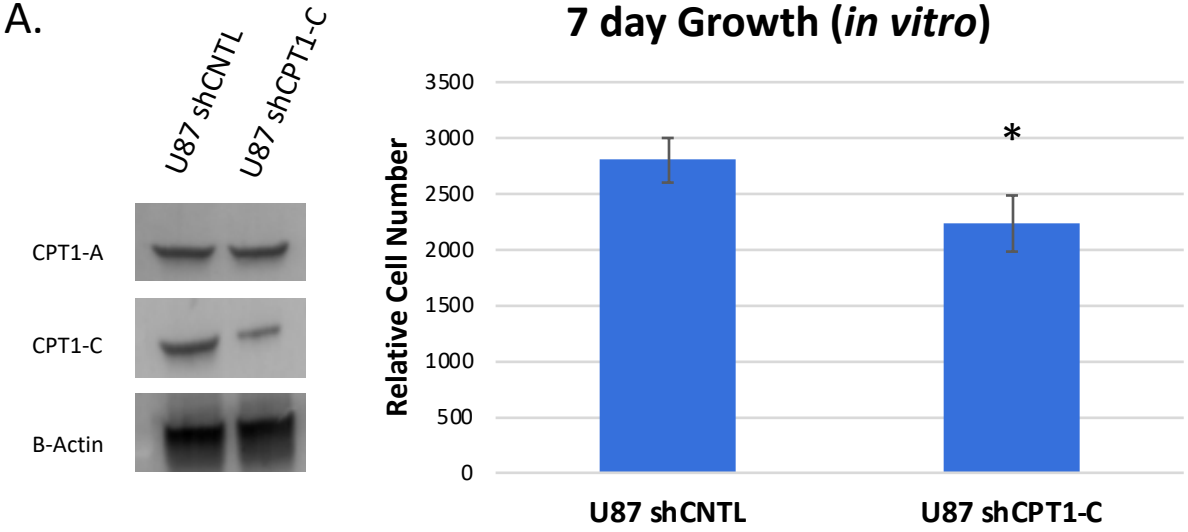

B.

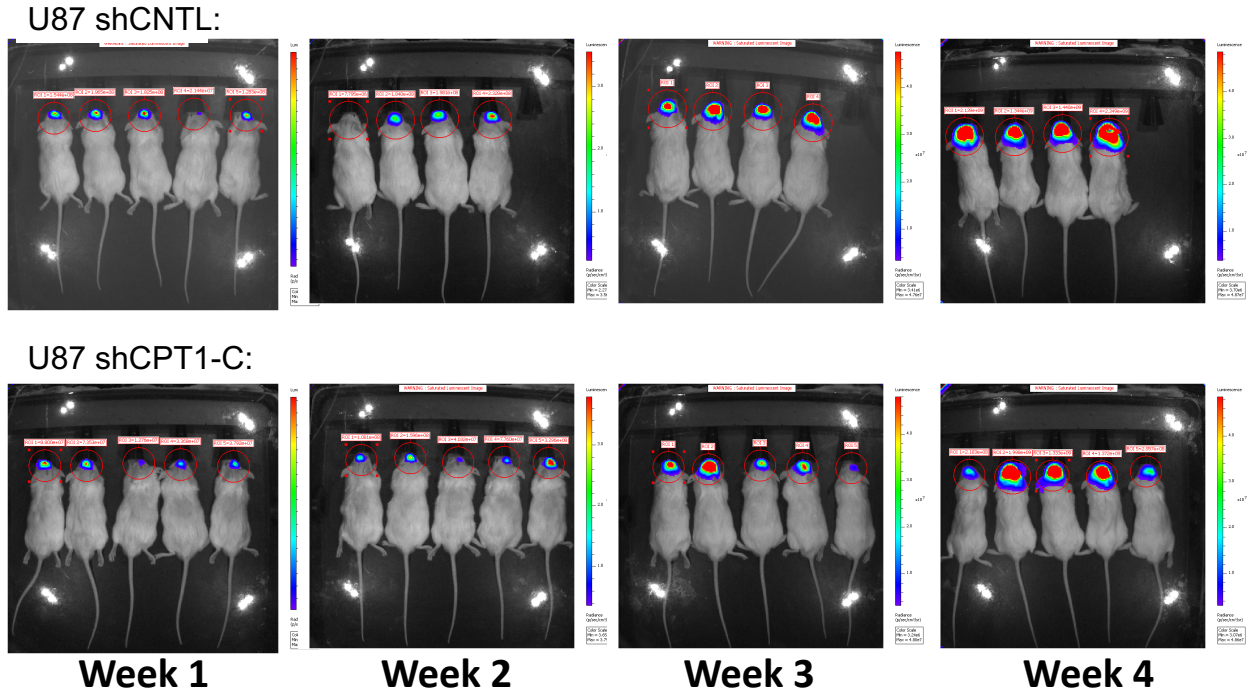

C.

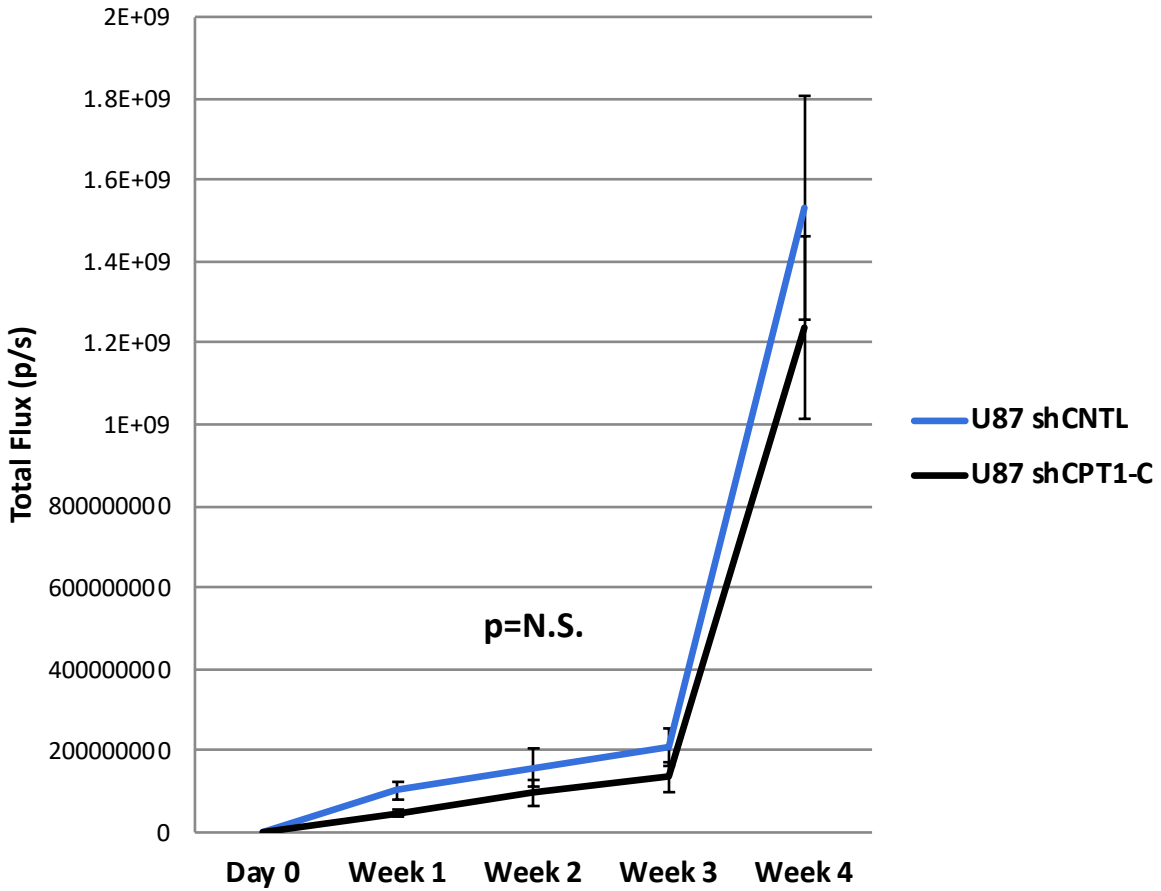

Supplementary Figure 3.

Relative Amounts of TCA cycle metabolites: (p = N.S. for all metabolites)

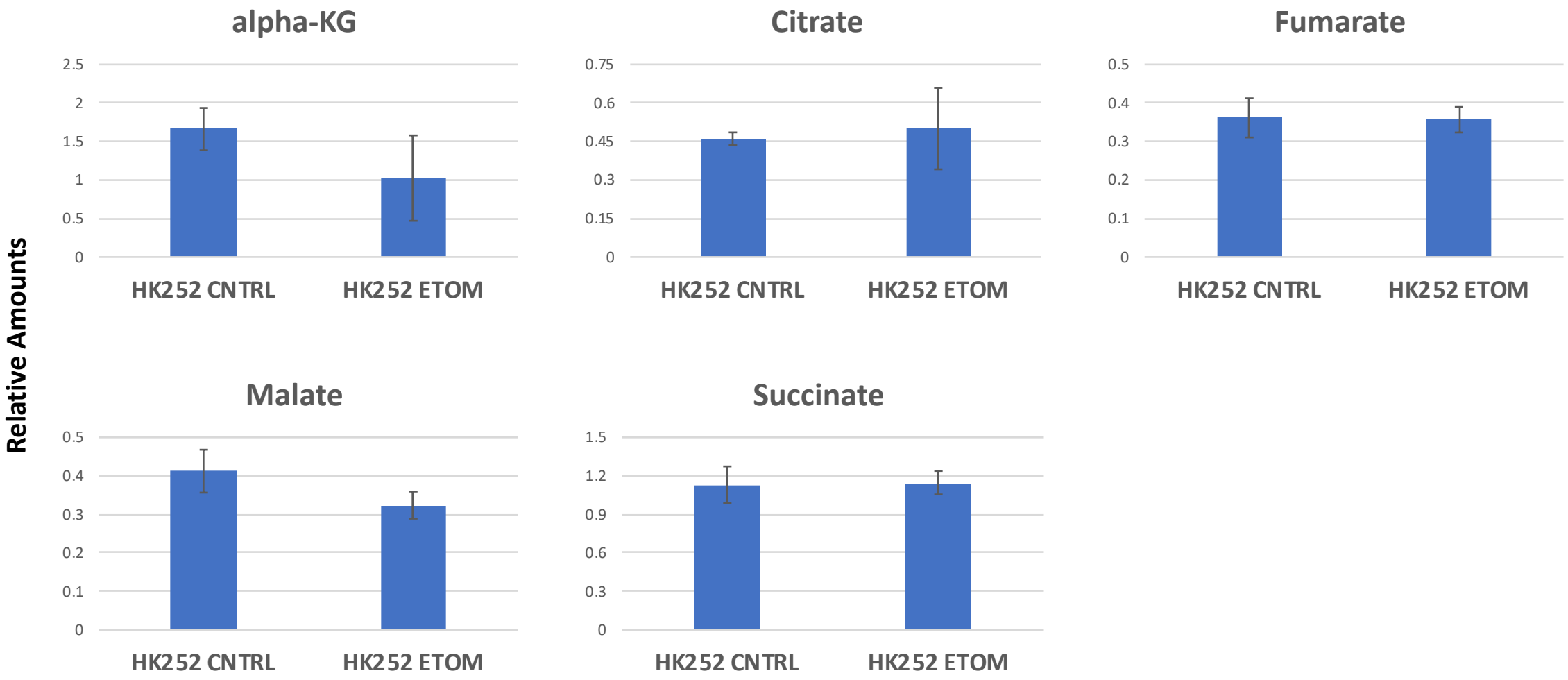

Supplementary Table 1.

Significantly different Metabolites (p<0.05): (* indicates increased levels with ETOM)

	TCA Cycle	Pentose Phosphate	Nucleotide Metabolism	Amino Acid Metabolism	Fatty Acid/Lipid Metabolism	Currency	Other
Fractional Contribution	Aconitate	SAM	5M-adenosine	Asn	Ac-carnitine	Acetyl-CoA	GlcN-6P*
	Cit		ATP	Asp	CDP	ATP	HMG-CoA
	Fum		C	Pro	CDP-EtA	GSH	
	Lac		CMP	P-Ser	Palmitate*	GSSG	
	Mal		CTP				
	Succ		Cytosine				
			Hypoxanthine				
	Gln		Orotidine				
	Glu		UDP				
			UDP-Glc				
			UDP-GlcNAc				
			UMP				
			UTP				
Relative Amounts	a-KG	Cystathionine	ATP	Ala	Ac-carnitine	ATP	GlcN-6P
	Cit	G6P-F6P	dATP	Pro	P-Choline	Creatine	4-OH-PheLac
	Fum	IMP*	CDP	Ser	P-EtA	NADH	Inositol
	Aconitate	R5P*	CTP	Thr		AMP/ATP Ratio*	Vit-C
			GTP	Citrulline			
	Gln		UTP	2-Methylpropanoyl-CoA			
	Glu		Orotidine				
			C*				
			Cytosine*				
			G*				

Supplementary Table 2.

Significantly different Metabolites (p<0.05): (* indicates increased levels with ETOM)

Fractional Contribution

TCA Cycle	Nucleotide Metabolism	Amino Acid Metabolism	Fatty Acid/Lipid Metabolism	Currency	Other
Aconitate	A	Asn	Ac-carnitine	Acetyl-CoA	GlcNAc-6P
Cit	Adenine	Asp	CDP	ATP	
Mal	ATP	Arg*	CDP-EtA	GSH	
Succ	C	Homocysteine		GSSG	
2-HG	CMP	Pro			
Gln	CTP				
Glu	Cytosine				
	dG				
	Inosine				
	Orotidine				
	UDP				
	UDP-Glc				
	UDP-GlcNAc				
	UMP				
	UTP				

Relative Amounts

2-HG	Adenine*	2-Methylpropanoyl-CoA		Acetyl-CoA	F16BP
Glu	dA*	Gly		Creatine	G6P-F6P
	GMP			NADH	GlcN-6P
	Inosine*				GlcNAc-6P
	Orotate*				Pantothenate
					Sorbitol